

A family of toroidal diffusions with exact likelihood inference

Eduardo García-Portugués^{1,3} and Michael Sørensen²

Abstract

We provide a class of diffusion processes for continuous time-varying multivariate angular data with explicit transition probability densities, enabling exact likelihood inference. The presented diffusions are time-reversible and can be constructed for any pre-specified stationary distribution on the torus, including highly-multimodal mixtures. We give results on asymptotic likelihood theory allowing one-sample inference and tests of linear hypotheses for k groups of diffusions, including homogeneity. We show that exact and direct diffusion bridge simulation is possible too. A class of circular jump processes with similar properties is also proposed. Several numerical experiments illustrate the methodology for the circular and two-dimensional torus cases. The new family of diffusions is applied (i) to test several homogeneity hypotheses on the movement of ants and (ii) to simulate bridges between the three-dimensional backbones of two related proteins.

Keywords: Angular data; Diffusion bridges; Stochastic processes; Torus.

1 Introduction

The modelling of time-varying angular observations on the circle $\mathbb{T}^1 := [0, 2\pi)$, with 0 and 2π identified, has been mainly focused on processes in discrete time (see Pewsey and García-Portugués, 2021, Section 10), with some seminal contributions being the Markov process of Wehrly and Johnson (1980) and the autoregressive processes of Breckling (1989) and Fisher and Lee (1994); see Harvey et al. (2024) for a recent score-driven approach to the latter.

One of the first continuous-time processes on \mathbb{T}^1 is the *von Mises process* by Kent (1975). The model describes the evolution of an angle $\{\Theta_t\} \subset \mathbb{T}^1$ by the stochastic differential equation

$$d\Theta_t = \frac{\sigma^2 \kappa}{2} \sin(\mu - \Theta_t) dt + \sigma dW_t, \quad (1)$$

where $\{W_t\}$ is a Wiener process, $\kappa \geq 0$ controls the strength of the drift towards $\mu \in [0, 2\pi)$, and $\sigma > 0$ is the diffusion coefficient. This Ornstein–Uhlenbeck-like process is ergodic with the von Mises distribution being its stationary distribution. The von Mises process has been applied in mathematical biology and physics, see, e.g., Hill and Häder (1997), Codling and Hill (2005), and Frank (2005, Section 5.3.3). Unlike the Ornstein–Uhlenbeck process, no closed-form expression for the transition probability density of (1) is known, which hampers likelihood-based inference.

García-Portugués et al. (2019) generalized the diffusion (1) to *Langevin diffusions* on the p -dimensional torus $\mathbb{T}^p = [0, 2\pi)^p$, $p \geq 1$. These processes are time-reversible, ergodic, and can be defined by any differentiable probability density function on \mathbb{T}^p (in particular, a wrapped normal density) that acts as the stationary density. However, the transition probability density is not explicitly known for the studied Langevin diffusions, with likelihood-based estimation requiring either expensive numerical solutions of the Kolmogorov’s forward equation, faster but less accurate pseudo-likelihoods, or more precise likelihood approximations that are specific to the wrapped normal diffusion. Golden et al. (2017) used the bivariate wrapped normal diffusion for their hidden Markov

¹Department of Statistics, Carlos III University of Madrid (Spain).

²Department of Mathematical Sciences, University of Copenhagen (Denmark).

³Corresponding author. e-mail: edgarcia@est-econ.uc3m.es.

model for protein structure evolution because of its faster and more accurate estimation within the available time-reversible and ergodic diffusions on the torus.

In the present paper, we make several contributions towards advancing diffusion models on the circle and torus, particularly targeting the lack of exact likelihood inference. Our main contribution is a family of diffusion processes on the torus for which closed-form expressions for the transition probability density functions can be given, implying that the likelihood function is explicitly known. The new family is constructed through a transformation argument specific to the geometry of \mathbb{T}^p , which we present first in Section 2 for the (technically easier) case $p = 1$ and then in Section 3 for $p \geq 1$. The diffusions in the new family are time-reversible and ergodic, and can have any differentiable density on the torus as the stationary density while maintaining the closed-form nature of the transition density. We derive asymptotic likelihood theory for samples observed at discrete times, both for the one sample case and for linear hypotheses in the case of k groups, in Section 4. The asymptotic results are validated with several numerical experiments. The new family of diffusions allows exact bridge simulation too, for which we give a direct algorithm in Section 5. We take a new direction in Section 6 to adapt the construction technique to produce jump processes on the circle with a given stationary distribution, analytic likelihood function, and exact bridge simulation. Finally, we give two in-depth biological applications of the new diffusion inferential toolbox in Section 7. The first uses homogeneity tests to investigate the effect of several factors on the circular ant movement induced by wall-following behaviour. The second exploits diffusion bridges to generate data-driven bridges between the protein backbones of a calcium-free calmodulin and a Ca^{2+} -calmodulin, using the dihedral-pairs representation of proteins.

2 Circular case

We consider the time-homogeneous diffusion given by the stochastic differential equation

$$dX_t = -\frac{\sigma^2 f'(X_t)}{2f(X_t)^3} dt + \frac{\sigma}{f(X_t)} dW_t, \quad (2)$$

where $\{W_t\}$ is a Wiener process, $\sigma > 0$ is a volatility coefficient, and $f : \mathbb{R} \rightarrow \mathbb{R}^+$ is a differentiable *circular* probability density function, that is, a function satisfying (i) $f(x + 2k\pi) = f(x)$ for any $x \in \mathbb{R}$ and $k \in \mathbb{Z}$ and (ii) $\int_0^{2\pi} f(\theta) d\theta = 1$. The wrapping of $\{X_t\}$ by the 2π -modulus operator produces the diffusion $\Theta_t = X_t \bmod 2\pi$, which (by definition) solves the stochastic differential equation

$$d\Theta_t = -\frac{\sigma^2 f'(\Theta_t)}{2f(\Theta_t)^3} dt + \frac{\sigma}{f(\Theta_t)} dW_t \quad (3)$$

on the circle $\mathbb{T}^1 = [0, 2\pi)$. The diffusion (2) is not ergodic. Its speed measure is infinite, so no stationary density exists. However, the wrapped process (3) is ergodic. The solution to (3) with $\Theta_0 = \theta_0 \in \mathbb{T}^1$ is given by

$$\Theta_t = F^{-1}(\sigma W_t + F(\theta_0)) \bmod 2\pi, \quad (4)$$

where $F : \mathbb{R} \rightarrow \mathbb{R}$, $F(x) := \int_0^x f(s) ds$, is a circular cumulative distribution function. Particularly, F is a one-to-one function verifying $F(x) = F(x \bmod 2\pi) + \lfloor x/(2\pi) \rfloor$ and having inverse $F^{-1}(y) = F^{-1}(y \bmod 1) + 2\pi \lfloor y \rfloor$, for all $x, y \in \mathbb{R}$. That F is a *circular* distribution function makes a remarkable difference with respect to the regular (linear) case. Indeed, if g is a regular density on \mathbb{R} with associated distribution function $G : \mathbb{R} \rightarrow [0, 1]$, then $G^{-1}(\sigma W_t + G(x_0))$ is an *explosive* solution for the diffusion (2) in which f is replaced by g , as $\sigma W_t + G(x_0)$ will eventually exit $[0, 1]$.

The following result collects the main properties of $\{\Theta_t\}$, in particular the transition probability density, i.e., the density of $\Theta_{t_2} \mid \Theta_{t_1} = \theta_1$. Proofs of all results can be found in the Appendix.

Proposition 2.1. Define $\Theta_t := F^{-1}(\sigma W_t + F(\theta_0)) \bmod 2\pi$, $t > 0$. Then:

i. $\{\Theta_t\}$ solves (3) with $\Theta_0 = \theta_0 \in \mathbb{T}^1$.

ii. For $t_2 > t_1 > 0$ and $\theta_1 \in \mathbb{T}^1$, the transition probability density of $\{\Theta_t\}$ is

$$p_{t_2-t_1}(\theta_2 | \theta_1) = 2\pi f_{\text{WN}}(2\pi F(\theta_2); 2\pi F(\theta_1), 4\pi^2(t_2 - t_1)\sigma^2) f(\theta_2), \quad \theta_2 \in \mathbb{T}^1, \quad (5)$$

where $f_{\text{WN}}(\theta; \mu, \sigma^2) := \sum_{k \in \mathbb{Z}} \phi_{\sigma^2}(\theta - \mu + 2k\pi)$ is the wrapped normal density, with $\phi_{\sigma^2}(\cdot)$ being the density of $\mathcal{N}(0, \sigma^2)$.

iii. $\{\Theta_t\}$ is ergodic with stationary density f and is time-reversible.

Some comments on the connections of diffusion (3) with other processes follow. First, it is easy to check that (3) is a Langevin diffusion on the circle (García-Portugués et al., 2019, Section 2) with variable diffusion coefficient given by σ/f and stationary density f . This variable diffusion coefficient also relates (3) to Roberts and Stramer (2002)'s Langevin *tempered* diffusions used to simulate from densities with untractable normalizing constants. Indeed, in (3) f can be replaced with an unnormalized density $f^* \propto f$ and still produce an ergodic diffusion with stationary density f , as the normalizing constant is absorbed by σ . There is also an interesting relation of the diffusion (3) to Wehrly and Johnson (1980)'s (discrete-time) Markov process on the circle, as (5) has a similar structure to the transition probability density in Wehrly and Johnson (1980)'s Equation (3). Additionally, the transformation (4) leading to (3) resembles that in Forman and Sørensen (2014), which is based on transforming a process X_t with stationary distribution function Π into $\tau(X_t)$ with $\tau := G^{-1} \circ \Pi$ and G a target stationary distribution function. However, the construction (4) cannot be cast in terms of τ as $\{W_t\}$ is not ergodic and, if replacing it with an ergodic process in $[0, 1]$, the transformation would yield a diffusion on $[0, 2\pi)$ with dynamics that do not allow it to move freely around the circle, as a barrier would be created at $0 \equiv 2\pi$.

Some notable examples of (3) follow.

Example 2.1 (Circular Brownian motion). For the circular uniform density $f \equiv 1/(2\pi)$, (3) becomes $d\Theta_t = \tilde{\sigma} dW_t$, the Brownian motion on the circle with volatility $\tilde{\sigma} := 2\pi\sigma$. This volatility gives a useful reference to compare the scale of σ for a non-uniform density f .

Example 2.2 (A von Mises diffusion). The von Mises distribution $\text{vM}(\mu, \kappa)$ has density $f_{\text{vM}}(\theta; \mu, \kappa) := (2\pi I_0(\kappa))^{-1} \exp\{\kappa \cos(\theta - \mu)\}$, where I_0 is the modified Bessel function of the first kind and zeroth order. Thus (3) has the form

$$d\Theta_t = \frac{\sigma^2 \kappa \sin(\Theta_t - \mu)}{2 \exp\{2\kappa \cos(\Theta_t - \mu)\}} dt + \frac{\sigma}{\exp\{\kappa \cos(\Theta_t - \mu)\}} dW_t \quad (6)$$

if the normalizing constant is absorbed in σ . The diffusion (6) shares with (1) the same stationary density $\text{vM}(\mu, \kappa)$, yet the latter does not have a known transition probability density. Besides, in (1) the stationary distribution is caused by the drift only, while in (6) it is the combined effect of the drift and the diffusion coefficient.

Example 2.3 (A wrapped Cauchy diffusion). The Wrapped Cauchy distribution $\text{WC}(\mu, \rho)$ has density $f_{\text{WC}}(\theta; \mu, \rho) := (2\pi)^{-1} (1 - \rho^2) (1 + \rho^2 - 2\rho \cos(\theta - \mu))^{-1}$. This density follows by transforming with a 2π -modulus the Cauchy distribution $\text{C}(\mu, \sigma^2)$ with density $f_{\text{C}}(x; \mu, \sigma^2) := \sigma\pi^{-1} ((x - \mu)^2 + \sigma^2)^{-1}$. Specifically, $f_{\text{WC}}(\theta; \mu, \rho) = \sum_{k \in \mathbb{Z}} f_{\text{C}}(\theta + 2k\pi; \mu, \sigma^2)$, with $\rho := e^{-\sigma}$. Absorbing the normalizing constant in σ , (3) produces a diffusion with stationary distribution $\text{WC}(\mu, \rho)$:

$$d\Theta_t = \sigma^2 \rho \sin(\Theta_t - \mu) (1 + \rho^2 - 2\rho \cos(\Theta_t - \mu))^2 dt + \sigma (1 + \rho^2 - 2\rho \cos(\Theta_t - \mu)) dW_t.$$

Figure 1 shows the multimodal transition probability densities of the diffusions in Examples 2.2–2.3, as well as for a diffusion given by a mixture of von Mises densities. The transition probability densities stabilize about the stationary density.

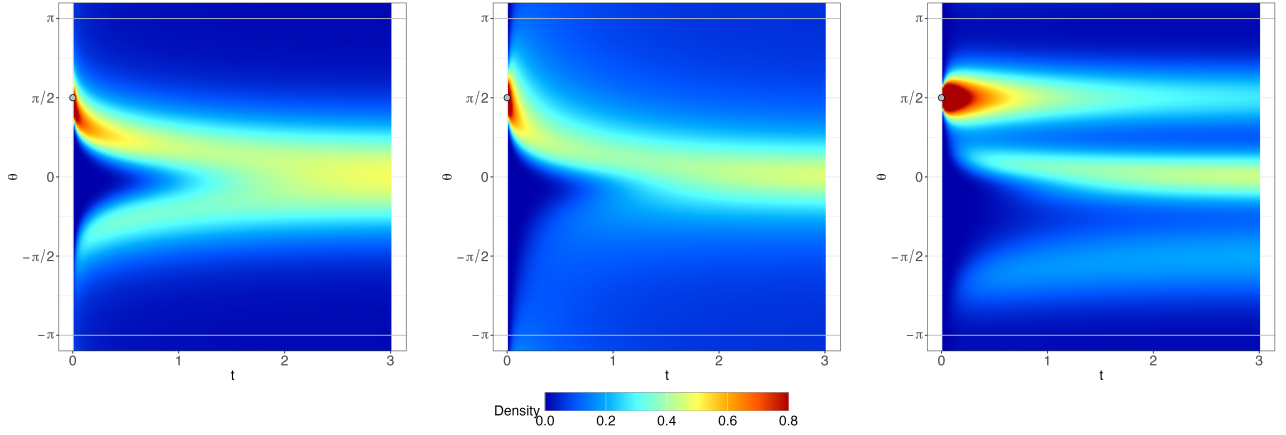


Figure 1: Temporal evolution of the transition probability density $p_t(\cdot \mid \theta_0)$ for three circular diffusions (3). From left to right, the diffusions are given by the distributions $\text{vM}(0, 2)$, $\text{WC}(0, 0.5)$, and the mixture $0.4\text{vM}(0, 8) + 0.3\text{vM}(-\pi/2, 3) + 0.3\text{vM}(\pi/2, 5)$. In all the plots, $\theta_0 = \pi/2$, $T = 3$, and $\sigma = 0.25$.

3 Toroidal case

The circular diffusion (3) can be extended to the p -dimensional torus, $\mathbb{T}^p = [0, 2\pi)^p$, $p \geq 1$, with 0 and 2π again identified. In analogy with the case $p = 1$, we start with a differentiable toroidal density f , i.e. a differentiable function $f : \mathbb{R}^p \rightarrow \mathbb{R}^+$ such that (i) $f(\mathbf{x} + 2\mathbf{k}\pi) = f(\mathbf{x})$ for all $\mathbf{x} \in \mathbb{R}^p$ and $\mathbf{k} \in \mathbb{Z}^p$ and (ii) $\int_{\mathbb{T}^p} f(\boldsymbol{\theta}) d\boldsymbol{\theta} = 1$. The joint toroidal distribution function $F(\mathbf{x}) := \int_0^{\mathbf{x}} f(\mathbf{s}) d\mathbf{s}$ does not provide a one-to-one function of \mathbb{R}^p onto itself. Instead we use Rosenblatt (1952)'s transformation to yield a one-to-one map $R : \mathbb{R}^p \rightarrow \mathbb{R}^p$. Define the conditional densities $f_j(x_j \mid x_1, \dots, x_{j-1}) = f(x_1, \dots, x_j) / f(x_1, \dots, x_{j-1})$ (with a slight abuse of notation for the marginal distribution). Clearly, $f_j(x_j + 2k_j\pi \mid x_1 + 2k_1\pi, \dots, x_{j-1} + 2k_{j-1}\pi) = f_j(x_j \mid x_1, \dots, x_{j-1})$ for all $\mathbf{x} \in \mathbb{R}^j$ and $\mathbf{k} \in \mathbb{Z}^j$, $j = 2, \dots, p$. Now, a one-to-one map $R : \mathbb{R}^p \rightarrow \mathbb{R}^p$ is given by

$$R(\mathbf{x}) := (F_1(x_1), F_2(x_2 \mid x_1), \dots, F_p(x_p \mid x_1, \dots, x_{p-1}))',$$

where F_1 is the first marginal distribution function of F , and $F_j(x_j \mid x_1, \dots, x_{j-1}) = \int_0^{x_j} f(s \mid x_1, \dots, x_{j-1}) ds$, $j = 2, \dots, p$. Let R^{-1} denote the inverse function, which for $p = 2$ has the form $R^{-1}(\mathbf{y}) = (F_1^{-1}(y_1), F_2^{-1}(y_2 \mid F_1^{-1}(y_1)))'$. As defined, R is a one-to-one map satisfying $R(\mathbf{x}) = R(\mathbf{x} \bmod 2\pi) + \lfloor \mathbf{x}/(2\pi) \rfloor$ and $R^{-1}(\mathbf{y}) = R^{-1}(\mathbf{y} \bmod 1) + 2\pi \lfloor \mathbf{y} \rfloor$, for all $\mathbf{x}, \mathbf{y} \in \mathbb{R}^p$, where the modulus and floor functions are applied componentwise.

We define the extension of the circular diffusion (3) to \mathbb{T}^p as

$$d\boldsymbol{\Theta}_t = \frac{1}{2} \begin{pmatrix} \text{tr}[\boldsymbol{\Sigma}(\mathbf{H}\mathbf{R}_1^{-1})(R(\boldsymbol{\Theta}_t))] \\ \vdots \\ \text{tr}[\boldsymbol{\Sigma}(\mathbf{H}\mathbf{R}_p^{-1})(R(\boldsymbol{\Theta}_t))] \end{pmatrix} dt + (\mathbf{D}\mathbf{R}^{-1})(R(\boldsymbol{\Theta}_t))\boldsymbol{\Sigma}^{1/2}d\mathbf{W}_t, \quad (7)$$

which is obtained by wrapping the diffusion $\{\mathbf{X}_t\}$ analogously defined on \mathbb{R}^p . Above, \mathbf{D} and \mathbf{H} stand for the Jacobian matrix and Hessian matrix operators, $\boldsymbol{\Sigma}$ is a covariance matrix, and $\{\mathbf{W}_t\}$ is a standard p -variate Wiener process. Note that the first q coordinates of the drift vector depend only on the first q coordinates of $\boldsymbol{\Theta}_t$, and that the matrix $(\mathbf{D}\mathbf{R}^{-1})(R(\boldsymbol{\Theta}_t))$ is a lower triangular matrix. When $p = 2$ and $\boldsymbol{\Sigma} = \sigma^2 \mathbf{I}_2$, with \mathbf{I}_p denoting the $p \times p$ identity matrix, (7) simplifies to

$$\begin{pmatrix} d\Theta_{1,t} \\ d\Theta_{2,t} \end{pmatrix} = -\frac{\sigma^2}{2} \begin{pmatrix} f_1'(\Theta_{1,t})(f_1(\Theta_{1,t}))^{-3} \\ f_2'(\Theta_{2,t} \mid \Theta_{1,t})(f_2(\Theta_{2,t} \mid \Theta_{1,t}))^{-3} + b(\boldsymbol{\Theta}_t) \end{pmatrix} dt + \sigma \begin{pmatrix} (f_1(\Theta_{1,t}))^{-1} & 0 \\ -h(\boldsymbol{\Theta}_t) & (f_2(\Theta_{2,t} \mid \Theta_{1,t}))^{-1} \end{pmatrix} \begin{pmatrix} dW_{1,t} \\ dW_{2,t} \end{pmatrix}, \quad (8)$$

where $b(\Theta_t) = (\partial_{x_1} h(\Theta_t))(f_1(\Theta_{1,t}))^{-1} - (\partial_{x_2} h(\Theta_t))h(\Theta_t)$ and

$$h(x_1, x_2) := \frac{\partial_{x_1} F_2(x_2 | x_1)}{f(x_1, x_2)} = \frac{1}{f_1(x_1)f(x_1, x_2)} \left[\partial_{x_1}^2 F(x_1, x_2) - \frac{f'_1(x_1)}{f_1(x_1)} \partial_{x_1} F(x_1, x_2) \right].$$

The expression above follows by tedious but straightforward computations involving the implicit function theorem. A simple instance of (7) for $p \geq 2$ is when $F(\mathbf{x}) = F_1(x_1) \cdots F_p(x_p)$, which gives the drift-independent and volatility-dependent diffusion

$$d\Theta_t = \frac{1}{2} \begin{pmatrix} -\sigma_1^2 f'_1(\Theta_{1,t})(f_1(\Theta_{1,t}))^{-3} \\ \vdots \\ -\sigma_p^2 f'_p(\Theta_{p,t})(f_p(\Theta_{p,t}))^{-3} \end{pmatrix} dt + \text{diag}(f_1(\Theta_{1,t}), \dots, f_p(\Theta_{p,t}))^{-1} \Sigma^{1/2} d\mathbf{W}_t \quad (9)$$

for an unrestricted covariance matrix Σ .

The following result collects the main properties of $\{\Theta_t\}$.

Proposition 3.1. *Define $\Theta_t := R^{-1}(\Sigma^{1/2} \mathbf{W}_t + R(\theta_0)) \bmod 2\pi$, $t > 0$. Then:*

i. $\{\Theta_t\}$ solves (7) with $\Theta_0 = \theta_0 \in \mathbb{T}^p$.

ii. For $t_2 > t_1 > 0$ and $\theta_1 \in \mathbb{T}^p$, the transition probability density of $\{\Theta_t\}$ is

$$p_{t_2-t_1}(\theta_2 | \theta_1) = (2\pi)^p f_{\text{WN}}(2\pi R(\theta_2); 2\pi R(\theta_1), 4\pi^2(t_2 - t_1)\Sigma) f(\theta_2), \quad \theta_2 \in \mathbb{T}^p, \quad (10)$$

where $f_{\text{WN}}(\theta; \mu, \Sigma) := \sum_{\mathbf{k} \in \mathbb{Z}^p} \phi_{\Sigma}(\theta - \mu + 2\mathbf{k}\pi)$ is the multivariate wrapped normal density, with $\phi_{\Sigma}(\cdot)$ being the density of $\mathcal{N}_p(\mathbf{0}, \Sigma)$.

iii. $\{\Theta_t\}$ is ergodic with stationary density f and is time-reversible.

The examples below extend Examples 2.1–2.2. An analogous extension of Example 2.3 could be possible using the bivariate wrapped Cauchy model by Kato and Pewsey (2015), but such an extension is, to the best of the authors' knowledge, (currently) hampered by the absence of readily usable formulae for its conditional densities.

Example 3.1 (Toroidal Brownian motion). *For the toroidal uniform density $f \equiv 1/(2\pi)^p$, (9) yields the Brownian motion on \mathbb{T}^p with covariance matrix $\tilde{\Sigma} := (2\pi)^{2p}\Sigma$, since $d\Theta_t = \tilde{\Sigma}^{1/2} d\mathbf{W}_t$.*

Example 3.2 (A bivariate von Mises diffusion). *A random vector $(\Theta_1, \Theta_2)'$ on \mathbb{T}^2 has the bivariate (sine) von Mises distribution (Singh et al., 2002), $\text{BvM}(\mu_1, \mu_2, \kappa_1, \kappa_2, \lambda)$, if its density is*

$$f_{\text{BvM}}(\theta_1, \theta_2; \mu_1, \mu_2, \kappa_1, \kappa_2, \lambda) := C(\kappa_1, \kappa_2, \lambda) \exp\{\kappa_1 \cos(\theta_1 - \mu_1) + \kappa_2 \cos(\theta_2 - \mu_2) + \lambda \sin(\theta_1 - \mu_1) \sin(\theta_2 - \mu_2)\}, \quad (11)$$

where the normalizing constant is $C(\kappa_1, \kappa_2, \lambda)^{-1} = 4\pi^2 \sum_{m=0}^{\infty} \binom{2m}{m} (\lambda^2/(4\kappa_1\kappa_2))^m I_m(\kappa_1) I_m(\kappa_2)$ and $(\mu_1, \mu_2)' \in \mathbb{T}^2$, $\kappa_1, \kappa_2 \geq 0$, and $\lambda \in \mathbb{R}$. Define $\mu_{2\lambda}(\theta_1) := \mu_2 + \tan^{-1}((\lambda/\kappa_2) \sin(\theta_1 - \mu_1))$ and $\kappa_{2\lambda}(\theta_1) := [\kappa_2^2 + \lambda^2 \sin^2(\theta_1 - \mu_1)]^{1/2}$. The marginal and conditional densities of Θ_1 and $\Theta_2 | \Theta_1 = \theta_1$ are, respectively,

$$\begin{aligned} f_1(\theta_1) &= C(\kappa_1, \kappa_2, \lambda)^{-1} 2\pi I_0(\kappa_{2\lambda}(\theta_1)) \exp\{\kappa_1 \cos(\theta_1 - \mu_1)\}, \\ f_2(\theta_2 | \theta_1) &= f_{\text{vM}}(\theta_2; \mu_{2\lambda}(\theta_1), \kappa_{2\lambda}(\theta_1)), \end{aligned}$$

and can be readily plugged into (8).

Mixtures of bivariate von Mises distributions can also be used to define the diffusion (8). Figure 2 displays snapshots of the transition probability density of such diffusion for different times, showing the convergence to the stationary mixture density.

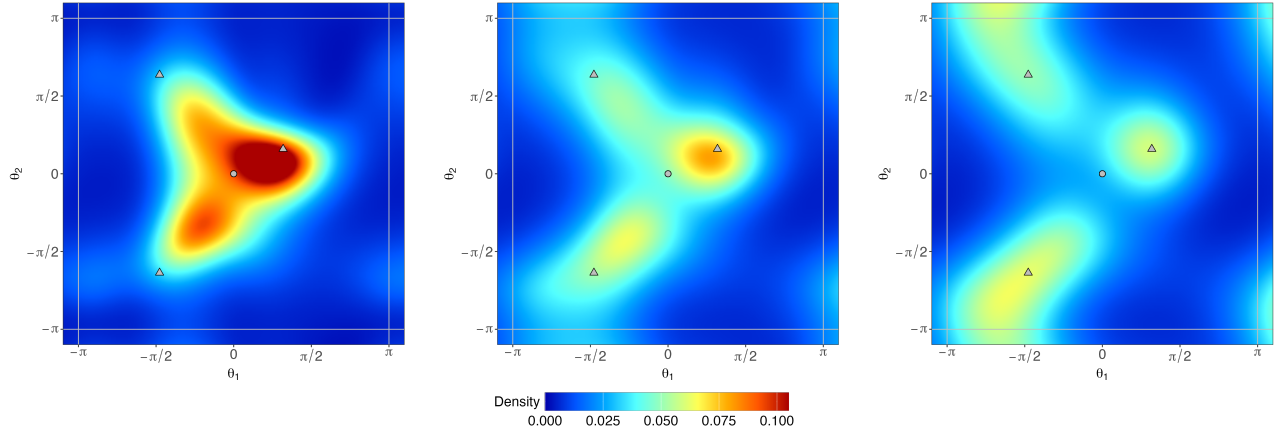


Figure 2: Temporal snapshots of the transition probability density $p_t(\cdot \mid \boldsymbol{\theta}_0)$ for $t = 0.2, 0.4, 1$ (from left to right) on the toroidal diffusion (8) given by the mixture $0.4\text{BvM}(-1.5, 2, 1, 1, -0.5) + 0.4\text{BvM}(-1.5, -2, 1, 1.5, 1) + 0.2\text{BvM}(1, 0.5, 2, 2, 0)$. In all the plots, $\boldsymbol{\theta}_0 = (0, 0)'$ (grey circle) and $\sigma = 0.5$. The grey triangles represent the mean of the mixture components.

4 Likelihood inference

4.1 One-sample inference

Suppose we have a parametrized class of circular densities f_β , $\beta \in B \subseteq \mathbb{R}^{q-1}$, and that we want to draw inference about the q -dimensional parameter $\boldsymbol{\xi}' = (\beta', \sigma) \in \Xi = B \times \mathbb{R}^+$ on the basis of the discrete-time observations $\Theta_0, \Theta_\Delta, \dots, \Theta_{n\Delta}$, $\Delta > 0$, of the diffusion given by (3). To simplify the exposition, we consider only the circular case. Similar results for the general toroidal case can be obtained in the same way.

By the Markov property, the log-likelihood function is

$$\ell_n(\boldsymbol{\xi}; \{\Theta_{i\Delta}\}_{i=0}^n) \equiv \ell_n(\boldsymbol{\xi}) = \sum_{i=1}^n \log p_\Delta(\Theta_{i\Delta}; \boldsymbol{\xi} \mid \Theta_{(i-1)\Delta}) \quad (12)$$

where

$$p_\Delta(\theta_2; \boldsymbol{\xi} \mid \theta_1) = f_\beta(\theta_2) \sum_{k \in \mathbb{Z}} \phi_{\sigma^2 \Delta}(h_k(\theta_1, \theta_2; \beta))$$

with $h_k(\theta_1, \theta_2; \beta) = F_\beta(\theta_2) - F_\beta(\theta_1) + k$. We denote $L_n(\boldsymbol{\xi}) := \exp(\ell_n)$ to the likelihood of $\boldsymbol{\xi}$.

Under the conditions of Theorem 4.1 below, the likelihood function is twice continuously differentiable with respect to $\boldsymbol{\xi}$. The score function is the vector-valued function

$$\partial_{\boldsymbol{\xi}} \ell_n(\boldsymbol{\xi}) = \sum_{i=1}^n \partial_{\boldsymbol{\xi}} \log p_\Delta(\Theta_{i\Delta}; \boldsymbol{\xi} \mid \Theta_{(i-1)\Delta}) \quad (13)$$

where, for $i = 1, \dots, q-1$,

$$\begin{aligned} \partial_{\xi_i} \log p_\Delta(\theta_2; \boldsymbol{\xi} \mid \theta_1) &= \partial_{\beta_i} \log f_\beta(\theta_2) \\ &\quad - \frac{\partial_{\beta_i} F_\beta(\theta_2) - \partial_{\beta_i} F_\beta(\theta_1)}{\sigma^2 \Delta} \frac{\sum_{k \in \mathbb{Z}} h_k(\theta_1, \theta_2; \beta) \phi_{\sigma^2 \Delta}(h_k(\theta_1, \theta_2; \beta))}{\sum_{k \in \mathbb{Z}} \phi_{\sigma^2 \Delta}(h_k(\theta_1, \theta_2; \beta))}. \end{aligned}$$

The last parameter coordinate ξ_q is σ and

$$\partial_\sigma \log p_\Delta(\theta_2; \boldsymbol{\xi} \mid \theta_1) = -\frac{1}{\sigma} + \frac{1}{\sigma^3 \Delta} \frac{\sum_{k \in \mathbb{Z}} h_k(\theta_1, \theta_2; \beta)^2 \phi_{\sigma^2 \Delta}(h_k(\theta_1, \theta_2; \beta))}{\sum_{k \in \mathbb{Z}} \phi_{\sigma^2 \Delta}(h_k(\theta_1, \theta_2; \beta))}.$$

Theorem 4.1. Assume the following conditions hold:

1. $\beta \mapsto f_\beta(\theta)$ and $\beta \mapsto F_\beta(\theta)$ are twice continuously differentiable for all $\theta \in \mathbb{T}^1$.
2. $f_\beta > 0$, and $\partial_\beta^k f_\beta$ and $\partial_\beta^k F_\beta$ are continuous functions of (β, θ) for $k = 0, 1, 2$.
3. The interior of Ξ is non-empty and contains ξ_0 , the true value of the parameter.
4. The covariance matrix of $\partial_\xi \log p_\Delta(\Theta_{2\Delta}; \xi \mid \Theta_\Delta)$ under the stationary distribution,

$$\mathcal{I}^\Delta(\xi) = \mathbb{E}_\xi(\partial_\xi \log p_\Delta(\Theta_{2\Delta}; \xi \mid \Theta_\Delta) \partial_\xi \log p_\Delta(\Theta_{2\Delta}; \xi \mid \Theta_\Delta)'), \quad (14)$$

is positive definite for all $\xi \in \Xi$. (\mathbb{E}_ξ denotes expectation with respect to the stationary distribution.)

Then, with a probability that goes to one as $n \rightarrow \infty$, a consistent maximum likelihood estimator $\hat{\xi}_n = (\hat{\beta}_n, \hat{\sigma}_n)'$ exists and is unique on any compact subset of Ξ containing ξ_0 . Moreover,

$$\sqrt{n}(\hat{\xi}_n - \xi_0) \xrightarrow{\mathcal{D}} \mathcal{N}_q(\mathbf{0}, \mathcal{I}^\Delta(\xi_0)^{-1}) \quad (15)$$

as $n \rightarrow \infty$, where $\mathcal{I}^\Delta(\xi_0)$ can be consistently estimated by $\mathcal{I}_n^\Delta(\hat{\xi}_n)$ with

$$\mathcal{I}_n^\Delta(\xi) = \frac{1}{n} \sum_{i=1}^n \partial_\xi \log p_\Delta(\Theta_{i\Delta}; \xi \mid \Theta_{(i-1)\Delta}) (\partial_\xi \log p_\Delta(\Theta_{i\Delta}; \xi \mid \Theta_{(i-1)\Delta}))'. \quad (16)$$

Finally, let $\xi' = (\xi^{(1)'}, \xi^{(2)'})$, where $\xi^{(1)}$ is q_1 -dimensional and $\xi^{(2)}$ is q_2 -dimensional ($q_1 + q_2 = q$). Let $Q_n := \sup_{\xi \in \Xi_0} L_n(\xi) / \sup_{\xi \in \Xi} L_n(\xi)$, with $\Xi_0 := \{\xi \in \Xi : \xi^{(2)} = \xi_0^{(2)}\}$. Then

$$-2 \log Q_n \xrightarrow{\mathcal{D}} \chi_{q_2}^2 \quad (17)$$

as $n \rightarrow \infty$, provided that $\mathcal{H}_0 : \xi^{(2)} = \xi_0^{(2)}$ holds.

The condition that the Fisher information (14) is satisfied if the coordinates of $\partial_\xi \log p_\Delta(\theta_2; \xi \mid \theta_1)$ are linearly independent functions of (θ_1, θ_2) . Note that the first term in the first $q - 1$ coordinates are the score function of the circular density f_β . Therefore, if the Fisher information for the model f_β , $\beta \in B$, is positive definite, then $\mathcal{I}^\Delta(\xi)$ is positive definite too, unless the derivatives of $\log \sum_{k \in \mathbb{Z}} \phi_{\sigma^2 \Delta}(h_k(\theta_1, \theta_2; \beta))$ depend on the derivatives of $\log f_\beta(\theta_2)$ in a rather pathological way.

The likelihood ratio test based on (17) rejects $\mathcal{H}_0 : \xi^{(2)} = \xi_0^{(2)}$ at the asymptotic significance level α when

$$-2 \log Q_n > \chi_{q_2; 1-\alpha}^2, \quad (18)$$

where $\chi_{q; \beta}^2$ denotes the order- β quantile of the chi-square distribution with q degrees of freedom. A possible use of this test is testing toroidal Brownian motionness against driftness and diffusionness: $\mathcal{H}_0 : \beta = \beta_0$, where β_0 is such that $f'_\beta \equiv 0$ vs. $\mathcal{H}_1 : \beta \neq \beta_0$. In diffusion (6), this corresponds to testing $\mathcal{H}_0 : \kappa = 0$ vs. $\mathcal{H}_1 : \kappa > 0$, while using the bivariate von Mises diffusion stemming from Example 3.2, it corresponds to $\mathcal{H}_0 : \kappa_1 = \kappa_2 = 0$ vs. $\mathcal{H}_1 : \kappa_1 > 0$ or $\kappa_2 > 0$. In these last two testing problems, the true parameter does not belong to the interior of the parameter space (third assumption in Theorem 4.1). However, through simulations we have corroborated that using the likelihood ratio test (18) still results in tests that respect the usual asymptotic nominal levels (Section 4.2). A deeper investigation of these and other boundary cases could be approached with the unrestricted maxima strategy of Feng and McCulloch (1992). Another interesting test is that of stationary independence, which in the bivariate von Mises diffusion is $\mathcal{H}_0 : \lambda = 0$ vs. $\mathcal{H}_1 : \lambda \neq 0$.

4.2 Numerical inference validation

Consider the von Mises diffusion given in Example 2.2, where $\xi' = (\xi^{(1)'}, \xi^{(2)'})$ with $\xi^{(1)'} = (\mu, \kappa)$ and $\xi^{(2)} = \sigma$. We address next an empirical validation of the inferential results in Theorem 4.1 for $\mathcal{H}_0 : \xi^{(1)} = \xi_0^{(1)}$. For that, we simulated $M = 10,000$ discretized trajectories $\{\Theta_{i\Delta}^{(j)}\}_{i=0}^n$ from (6) with $n = 50, 200$ and $\Delta = 0.5$, where $j = 1, \dots, M$. The data generation process (DGP) parameters are $\xi_k = (0, \kappa_k, 1/(2\pi))'$ with $\kappa_k = 1 + 0.10k$, $k = 0, 1, 2$. The initial $\Theta_0^{(j)}$'s were drawn from the stationary distribution $\text{vM}(0, \kappa_k)$. Simulation from (3) is trivial and exact from (4); in particular, it does not require an Euler-like discretization. The maximum likelihood estimators $\hat{\xi}_n$ were computed by numerically maximizing (12), using the stationary maximum likelihood estimates (García-Portugués et al., 2019, Section 3.1) as starting values. $\mathcal{I}^\Delta(\xi)$ was approximated by M Monte Carlo samples.

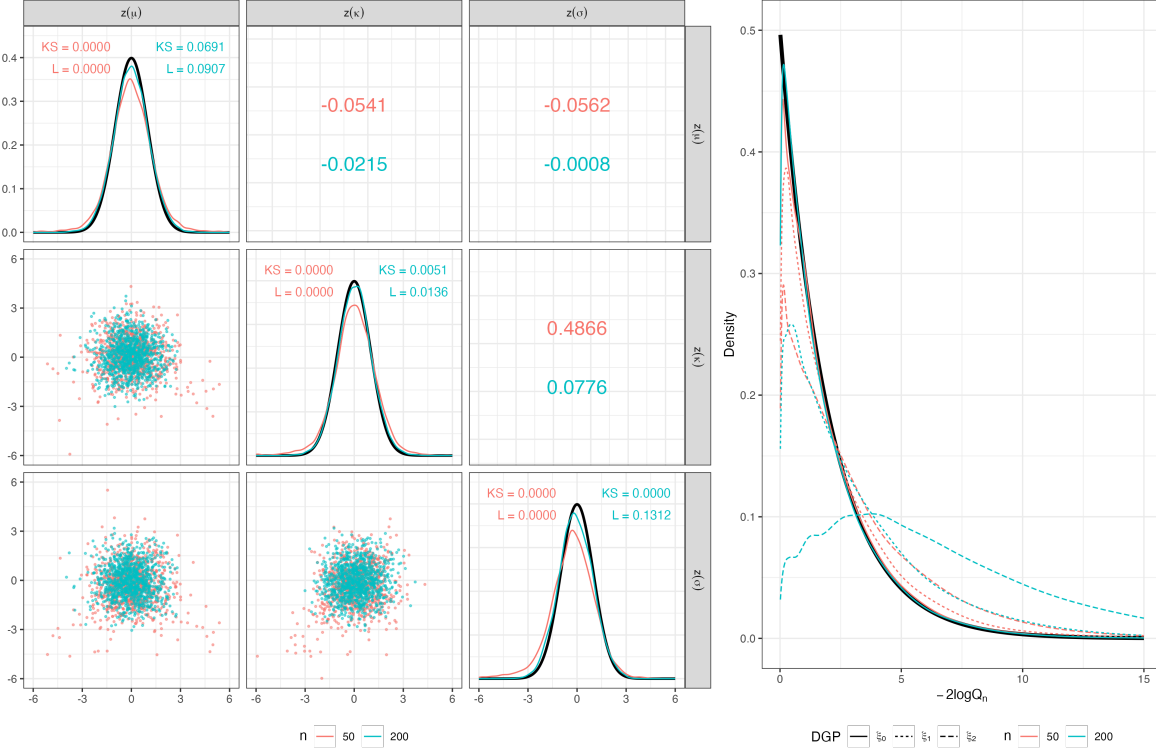


Figure 3: Empirical validation of Theorem 4.1 for $n = 50$ (red) and $n = 200$ (turquoise). The left plot shows a diagnostic on the multivariate normality of $z^{(j)} := \sqrt{n}\mathcal{I}^\Delta(\xi_0)^{1/2}(\hat{\xi}_n^{(j)} - \xi_0)$, $j = 1, \dots, M$, with $\hat{\xi}_n^{(j)}$ estimated with samples from the data generation process with $\xi = \xi_0$. The upper and lower panels show correlations and scatterplots, respectively, while central panels give the standard normal density (black), marginal kernel density estimators, and p -values of normality tests. The right plot displays the density of the χ_2^2 distribution (black) and the kernel density estimators of $-2\log Q_n$ under $\mathcal{H}_0 : \xi^{(1)} = \xi_0^{(1)}$ and $\mathcal{H}_1 : \xi^{(1)} = \xi_k^{(1)}$, $k = 1, 2$.

The left plot in Figure 3 shows the pairwise scatterplots of $z^{(j)} := \sqrt{n}\mathcal{I}^\Delta(\xi_0)^{1/2}(\hat{\xi}_n^{(j)} - \xi_0)$ (lower panels) for a subset of 2,000 observations. The only data generation process considered is that with ξ_0 . For $n = 50$ (red), non-normal dispersion patterns are evident, especially in the κ and σ components. This is also reflected in their correlations (upper panels). Also, the marginal kernel density estimators signal a deviation from the expected ϕ density (black), aligning with the p -values of the Kolmogorov–Smirnov (KS) test for $\mathcal{N}(0, 1)$ and the Lilliefors (L) test. Correlations and tests were computed from the whole sample $\{z^{(j)}\}_{j=1}^M$. When n increases to $n = 200$ (turquoise), the previous metrics improve and convergence towards a $\mathcal{N}_3(\mathbf{0}, \mathbf{I}_3)$ is evidenced, thus validating numerically (15). The bandwidths of the kernel density estimators were chosen with the rule-of-thumb selector.

The convergence in (17) under $\mathcal{H}_0 : \boldsymbol{\xi}^{(1)} = \boldsymbol{\xi}_0^{(1)}$ is neatly corroborated in the right plot in Figure 3 with the close match between the kernel density estimators of $\{-2\log Q_n^{(j)}\}_{j=1}^M$ and the density of the χ_2^2 distribution (black). The p -values of the KS test for χ_2^2 are 0.0159 ($n = 50$) and 0.1049 ($n = 200$). As expected, under $\mathcal{H}_1 : \boldsymbol{\xi}^{(1)} = \boldsymbol{\xi}_k^{(1)}$, $k = 1, 2$, the kernel density estimators diverge from the null χ_2^2 density at different paces controlled by the strength k of the deviation (line types) and the sample size n (colours), even though the divergence from \mathcal{H}_0 only happens in the κ component. The kernel density estimators in the plot were obtained through log-transformation and rule-of-thumb bandwidths.

A final validation concerns the empirical rejection rates of (18) under $\mathcal{H}_0 : \boldsymbol{\xi}^{(1)} = \boldsymbol{\xi}_0^{(1)}$. For the asymptotic significance levels $\alpha = 0.10, 0.05, 0.01$, these were: 0.1053, 0.0512, and 0.0109 ($n = 50$); 0.1014, 0.0502, and 0.0105 ($n = 200$). When testing the boundary hypothesis $\mathcal{H}_0 : \kappa = 0$ for the different data generation processes with $\boldsymbol{\xi} = (0, 0, 1/(2\pi))'$, the empirical rejection rates were: 0.0929, 0.0461, and 0.0100 ($n = 50$); 0.0965, 0.0477, and 0.0092 ($n = 200$). Except 0.0929, all the rejection rates are inside the asymptotic 95% confidence interval for α .

4.3 Test of linear hypotheses for k groups of diffusions

Consider k circular diffusions (3) with the same underlying parametric form for the density $f_{\boldsymbol{\beta}}$, $\boldsymbol{\beta} \in B \subseteq \mathbb{R}^{q-1}$, but with possibly different parameter values. Let there be N_j independent and identically distributed copies of each diffusion, with $j = 1, \dots, k$. The following uncoupled system of stochastic differential equations arises:

$$d\Theta_t^{(i,j)} = -\frac{\sigma_j^2 f'_{\boldsymbol{\beta}_j}(\Theta_t^{(i,j)})}{2f_{\boldsymbol{\beta}_j}(\Theta_t^{(i,j)})^3} dt + \frac{\sigma_j}{f_{\boldsymbol{\beta}_j}(\Theta_t^{(i,j)})} dW_t^{(i,j)}, \quad t \in [0, T_j], \quad (19)$$

where $i = 1, \dots, N_j$, $\boldsymbol{\beta}_j \in B$, and $\boldsymbol{\xi}'_j = (\boldsymbol{\beta}'_j, \sigma_j)' \in B \times \mathbb{R}^+$ collects the parameters of the j th diffusion. An instance of (19) is used in Section 7.1, where $\{\Theta_t^{(i,j)}\}$ represents the angles of movement of the i th ant in the j th group during an experiment lasting time T_j .

Given the discrete time observations $\{\Theta_{\nu\Delta_j}^{(i,j)}\}_{\nu,i,j=0,1,1}^{n_j, N_j, k}$, the log-likelihood function of the vector of parameters of (19), $\boldsymbol{\xi} = (\boldsymbol{\xi}'_1, \dots, \boldsymbol{\xi}'_k)' \in \Xi = (B \times \mathbb{R}^+)^k$, is

$$\ell_{\mathbf{n}, \mathbf{N}}(\boldsymbol{\xi}; \{\Theta_{\nu\Delta_j}^{(i,j)}\}_{\nu,i,j=0,1,1}^{n_j, N_j, k}) = \sum_{j=1}^k \sum_{i=1}^{N_j} \ell_{n_j}(\boldsymbol{\xi}_j; \{\Theta_{\nu\Delta_j}^{(i,j)}\}_{\nu=0}^{n_j}), \quad (20)$$

where $\mathbf{n} := (n_1, \dots, n_k)$ and $\mathbf{N} := (N_1, \dots, N_k)$, and where ℓ_{n_j} is given by (12).

We first give a result on the likelihood ratio test for general linear hypotheses for k groups of diffusions.

Theorem 4.2. *Assume conditions 1–3 from Theorem 4.1 hold, and that condition 4 holds for each $\mathcal{I}^{\Delta_j}(\boldsymbol{\xi})$, $j = 1, \dots, k$. Consider a subset of unrestricted parameters $A \subseteq \mathbb{R}^{\tilde{q}}$ ($\tilde{q} < kq$) and a $kq \times \tilde{q}$ -matrix \mathbf{M} of full rank \tilde{q} such that $\Xi_0 := \mathbf{M}A \subset \Xi$, where the notation $\mathbf{M}A = \{\mathbf{M}\mathbf{a} \mid \mathbf{a} \in A\}$ is used. Let $Q_{\mathbf{n}, \mathbf{N}} := \sup_{\boldsymbol{\xi} \in \Xi_0} L_{\mathbf{n}, \mathbf{N}}(\boldsymbol{\xi}) / \sup_{\boldsymbol{\xi} \in \Xi} L_{\mathbf{n}, \mathbf{N}}(\boldsymbol{\xi})$, with $L_{\mathbf{n}, \mathbf{N}} := \exp(\ell_{\mathbf{n}, \mathbf{N}})$. Then, provided that the hypothesis $\mathcal{H}_0 : \boldsymbol{\xi} \in \Xi_0$ holds,*

$$-2\log Q_{\mathbf{n}, \mathbf{N}} \xrightarrow{\mathcal{D}} \chi_{kq-\tilde{q}}^2 \quad (21)$$

as $n_1 N_1, \dots, n_k N_k \rightarrow \infty$ with $n_j N_j / (n_1 N_1) = O(1)$ for $j = 1, \dots, k$.

By essentially the same proof, a similar more general result can be proved for the likelihood ratio test for one linear hypothesis under another less restrictive linear hypothesis.

An important particular case is testing the homogeneity of subsets of parameters of ξ_j , $j = 1, \dots, k$, across the k groups. Let $\xi'_j = (\xi_j^{(1)'}, \xi_j^{(2)'})$, where $\xi_j^{(1)}$ is q_1 -dimensional and $\xi_j^{(2)}$ is q_2 -dimensional ($q_1 + q_2 = q$), for all $j = 1, \dots, k$. The hypothesis $\mathcal{H}_0 : \xi_1^{(2)} = \dots = \xi_k^{(2)}$ is of the type considered in Theorem 4.2 with $\Xi_0 := \{\xi \in \Xi : \xi_1^{(2)} = \dots = \xi_k^{(2)}\}$ and $\tilde{q} = kq_1 + q_2$. Therefore,

$$-2 \log Q_{n,N} \xrightarrow{\mathcal{D}} \chi_{(k-1)q_2}^2. \quad (22)$$

As an example, consider the von Mises diffusion with two groups. Here $\xi_j = (\mu_j, \kappa_j, \sigma_j)' \in [0, 2\pi) \times (0, \infty)^2$, $j = 1, 2$. Suppose we wish to test the hypothesis $\mathcal{H}_0 : \sigma_1 = \sigma_2$. The unrestricted parameters are then $(\mu_1, \kappa_1, \sigma_1, \mu_2, \kappa_2) \in A = [0, 2\pi) \times (0, \infty)^2 \times [0, 2\pi) \times (0, \infty)$ and

$$M = \begin{pmatrix} 1 & 0 & 0 & 0 & 0 \\ 0 & 1 & 0 & 0 & 0 \\ 0 & 0 & 1 & 0 & 0 \\ 0 & 0 & 0 & 1 & 0 \\ 0 & 0 & 0 & 0 & 1 \\ 0 & 0 & 1 & 0 & 0 \end{pmatrix}.$$

The likelihood ratio test based on (22) provides substantial flexibility. Within the von Mises diffusion (6), perhaps the most immediate case is the ANOVA-type test of equal stationary means ($\mathcal{H}_0 : \mu_1 = \dots = \mu_k$), which can be extended to the test of equal stationary distributions ($\mathcal{H}_0 : (\mu_1, \kappa_1) = \dots = (\mu_k, \kappa_k)$) or to the most stringent test of homogeneous diffusions ($\mathcal{H}_0 : (\mu_1, \kappa_1, \sigma_1) = \dots = (\mu_k, \kappa_k, \sigma_k)$). Besides, the likelihood ratio test in Theorem 4.1 can be straightforwardly adapted to test $\mathcal{H}_0 : \xi^{(1)} = \xi^{(2)}$ in a two-piece version of the circular diffusion (3) featuring a change point at time T_1 :

$$d\Theta_t^{(i)} = -\frac{\sigma_j^2 f'_{\beta_j}(\Theta_t^{(i)})}{2f_{\beta_j}(\Theta_t^{(i)})^3} dt + \frac{\sigma_j}{f_{\beta_j}(\Theta_t^{(i)})} dW_t^{(i)}, \quad j = \begin{cases} 1, & \text{if } t \in [0, T_1], \\ 2, & \text{if } t \in (T_1, T_2], \end{cases} \quad (23)$$

with $0 < T_1 < T_2$ and $i = 1, \dots, N$.

We conclude the section with a small numerical validation of Theorem 4.2 akin to that of Section 4.2. Let $k = 2$, $n_1 = n_2 = 50$, and $\Delta_1 = \Delta_2 = 0.5$. The data generation process of both groups are von Mises diffusions. The first has parameters $\xi_1 = (0, 1, 1/(2\pi))'$. The parameters of the second diffusion differ only in the concentration: $\xi_{2,a} = (0, 1 + a/10, 1/(2\pi))'$ for $a = 0, 1, \dots, 5$. We apply the likelihood ratio test for the null hypotheses and sample sizes described in Table 1 for $M = 10,000$ discretized trajectories $\{\Theta_{\ell\Delta_j}^{(i,j)}\}_{\ell,i,j=0,1,1}^{n_j, N_j, k}$.

As expected, Table 1 corroborates that: (i) the tests maintain the significance level, with the null rejection rates for $(N_1, N_2) = (10, 5)$ being within the asymptotic 95% confidence interval for α ; (ii) the tests for $\mathcal{H}_0 : \mu_1 = \mu_2$ and $\mathcal{H}_0 : \sigma_1 = \sigma_2$ are ‘blind’ against the considered alternative; (iii) the tests for $\mathcal{H}_0 : \kappa_1 = \kappa_2$, $\mathcal{H}_0 : (\kappa_1, \sigma_1) = (\kappa_2, \sigma_2)$ and $\mathcal{H}_0 : (\mu_1, \kappa_1) = (\mu_2, \kappa_2)$, and $\mathcal{H}_0 : (\mu_1, \kappa_1, \sigma_1) = (\mu_2, \kappa_2, \sigma_2)$ are decreasingly ordered in terms of power; (iv) the non-trivial powers increase with (N_1, N_2) (n_1 and n_2 are fixed).

5 Diffusion bridge simulation

By virtue of Proposition 3.1, simulating a diffusion bridge $\Theta_t \mid (\Theta_0 = \theta_0, \Theta_T = \theta_T)$ for (7) reduces to sampling a certain ‘winding number’ $\mathbf{K}_T \in \mathbb{Z}^p$ associated with θ_T , simulating the Brownian bridge $\mathbf{W}_t \mid (\mathbf{W}_0 = \mathbf{x}, \mathbf{X}_T = \mathbf{y})$ for certain initial and final values \mathbf{x} and \mathbf{y} , and applying a posterior wrapping. The following theorem makes this procedure precise.

Theorem 5.1. *Let $\{\Theta_t\}$ be the toroidal diffusion given by (7), $0 < t < T$, and consider $\theta_0, \theta_T \in \mathbb{T}^p$ and $0 < t_1 < \dots < t_n < T$.*

i. Simulate $\mathbf{K}_T \in \mathbb{Z}^p$ such that

$$\mathbb{P}[\mathbf{K}_T = \mathbf{k}] = \frac{\phi_{T\Sigma}(R(\boldsymbol{\theta}_T) - R(\boldsymbol{\theta}_0) + \mathbf{k})}{\sum_{\mathbf{m} \in \mathbb{Z}^p} \phi_{T\Sigma}(R(\boldsymbol{\theta}_T) - R(\boldsymbol{\theta}_0) + \mathbf{m})}, \quad \mathbf{k} \in \mathbb{Z}^p. \quad (24)$$

ii. Simulate independently $Z_{i,j} \sim \mathcal{N}(0, t_i - t_{i-1})$ for $i = 1, \dots, n+1$ and $j = 1, \dots, p$, with $t_0 = 0$ and $t_{n+1} = T$, and calculate

$$U_{i,j} = \sum_{m=1}^i Z_{m,j} - \frac{t_i}{T} \left(\sum_{m=1}^{n+1} Z_{m,j} - y_j \right) \quad (25)$$

for $i = 1, \dots, n$, $j = 1, \dots, p$, where $\mathbf{y} := \Sigma^{-1/2}(R(\boldsymbol{\theta}_T) - R(\boldsymbol{\theta}_0) + \mathbf{K}_T)$.

iii. Set $\mathbf{B}_i := R^{-1}(\Sigma^{1/2}\mathbf{U}_i + R(\boldsymbol{\theta}_0)) \bmod 2\pi$ with $\mathbf{U}_i = (U_{i,1}, \dots, U_{i,p})'$.

Then $(\mathbf{B}_1, \dots, \mathbf{B}_n)$ is distributed as $(\boldsymbol{\Theta}_{t_1}, \dots, \boldsymbol{\Theta}_{t_n}) \mid (\boldsymbol{\Theta}_0 = \boldsymbol{\theta}_0, \boldsymbol{\Theta}_T = \boldsymbol{\theta}_T)$.

By the Markov property and time-reversibility, the density of $\boldsymbol{\Theta}_t \mid (\boldsymbol{\Theta}_0 = \boldsymbol{\theta}_0, \boldsymbol{\Theta}_T = \boldsymbol{\theta}_T)$ is

$$p_t(\boldsymbol{\theta} \mid \boldsymbol{\Theta}_0 = \boldsymbol{\theta}_0, \boldsymbol{\Theta}_T = \boldsymbol{\theta}_T) = \frac{p_{T-t}(\boldsymbol{\theta} \mid \boldsymbol{\Theta}_0 = \boldsymbol{\theta}_T) p_t(\boldsymbol{\theta} \mid \boldsymbol{\Theta}_0 = \boldsymbol{\theta}_0) f(\boldsymbol{\theta}_T)}{p_T(\boldsymbol{\theta}_T \mid \boldsymbol{\Theta}_0 = \boldsymbol{\theta}_0) f(\boldsymbol{\theta})}, \quad 0 < t < T.$$

Figure 4 displays several bridges simulated using Theorem 5.1. The bridges join two pairs of initial-end points (grey circles and triangles) in three circular/toroidal diffusions with prescribed stationary densities. As expected, the sample paths show higher/lower volatility at low/high-density regions and honour the periodicity of the support.

(N_1, N_2)	Homogeneity	$a = 0$	$a = 1$	$a = 2$	$a = 3$	$a = 4$	$a = 5$
(3, 2)	Means	5.37	5.55	5.45	5.34	5.27	5.23
	Concentrations	5.38	9.50	21.27	39.65	59.25	75.59
	Volatilities	5.12	5.21	5.23	5.20	5.26	5.34
	Concs. & volas.	5.43	8.64	17.19	32.13	51.10	68.79
	Stationary distrs.	5.51	8.47	17.20	31.13	49.43	67.47
	Diffusions	5.53	7.83	15.04	27.46	44.90	62.43
(10, 5)	Means	4.98	5.04	5.12	5.02	4.96	5.11
	Concentrations	5.25	18.21	50.44	81.09	96.30	99.42
	Volatilities	5.22	5.24	5.27	5.23	5.10	5.13
	Concs. & volas.	5.19	14.07	40.85	74.06	93.03	98.91
	Stationary distrs.	5.17	13.56	40.05	73.03	92.51	98.65
	Diffusions	5.22	11.78	35.22	68.15	89.81	98.11

Table 1: Empirical rejection levels of null hypotheses of homogeneity for $k = 2$ groups using the likelihood ratio test based on (22). The case $a = 0$ represents equal data generation processes; $a > 0$ introduces a shift on the concentrations. All tests are performed at the asymptotic significance level $\alpha = 0.05$.

6 Circular jump processes with exact likelihood inference

The construction in the previous sections can also be applied to other Lévy processes. To demonstrate this, we present a particularly useful case based on the Cauchy process.

Let $\{V_t\}$ be a (symmetric) Cauchy process with scale parameter σ . Then $V_{t_2} - V_{t_1}$ is $C(0, ((t_2 - t_1)\sigma)^2)$ -distributed for $t_2 > t_1 > 0$, where $C(\mu, \sigma^2)$ denotes the Cauchy distribution given in Example

2.3. As in Section 2, let $f : \mathbb{R} \rightarrow \mathbb{R}^+$ be a given circular density, and let $F : \mathbb{R} \rightarrow \mathbb{R}$ be the associated circular distribution function, and define the jump process

$$\Theta_t = F^{-1}(V_t + F(\theta_0)) \mod 2\pi. \quad (26)$$

It follows by arguments analogous to those given in the diffusion case that the transition probability density of $\{\Theta_t\}$ is

$$p_t(\theta_2 | \theta_1) = \frac{(1 - \rho_t(\sigma)^2)f(\theta_2)}{1 + \rho_t(\sigma)^2 - 2\rho_t(\sigma)\cos(2\pi(F(\theta_2) - F(\theta_1)))},$$

where $\rho_t(\sigma) := e^{-2\pi t\sigma}$. The process is time-reversible and ergodic with stationary density f . The asymptotic results on likelihood inference in Theorem 4.1 hold for the circular jump process under the same conditions as in Theorem 4.1.

An algorithm for simulating a circular jump process bridge similar to the one in Theorem 5.1 can be obtained by using that a Cauchy process is a stochastic time transformation of a Wiener process, see Applebaum (2009, Section 1.3). Let $\{\tilde{W}_t\}$ be a Wiener process with infinitesimal variance $2\sigma^2$, and $\{S_t\}$ an independent Lévy subordinator, i.e., $\{S_t\}$ is a non-negative, increasing Lévy process, where S_t is Lévy-distributed with scale parameter $\beta = t^2/2$. Then $V_t = \tilde{W}_{S_t}$ is a Cauchy process with scale parameter σ . If $X \sim \mathcal{N}(0, \beta^{-1})$, then X^{-2} is Lévy distributed with scale parameter β .

Theorem 6.1. *Let $\{\Theta_t\}$ be the circular jump process given by (26), $0 < t < T$, and consider $\theta_0, \theta_T \in \mathbb{T}^1$ and $0 = t_0 < t_1 < \dots < t_n < t_{n+1} = T$.*

i. Simulate $K_T \in \mathbb{Z}$ such that

$$\mathbb{P}[K_T = k] = \frac{T\sigma[1 + \rho_T(\sigma)^2 - 2\rho_T(\sigma)\cos(2\pi(F(\theta_T) - F(\theta_0)))]}{\pi(1 - \rho_T(\sigma)^2)[(F(\theta_T) - F(\theta_0) + k)^2 + (T\sigma)^2]}, \quad k \in \mathbb{Z}. \quad (27)$$

ii. Simulate independently the vector (A_1, \dots, A_{n+1}) with joint density

$$f_A(a_1, \dots, a_{n+1}) = \frac{\phi_{2\sigma^2(a_1^{-2} + \dots + a_{n+1}^{-2})}(y)}{f_C(y; 0, (T\sigma)^2)} \prod_{i=1}^{n+1} \phi_{2\Delta_i^{-2}}(a_i), \quad (28)$$

where $y := F(\theta_T) - F(\theta_0) + K_T$, $\Delta_i := t_i - t_{i-1}$, and f_C denotes the density of the Cauchy distribution, see Example 2.3.

iii. Conditionally on A_1, \dots, A_{n+1} , simulate independently $Z_j \sim \mathcal{N}(0, 2\sigma^2 A_j^{-2})$ for $j = 1, \dots, n+1$ and calculate

$$U_i = \sum_{j=1}^i Z_j - \frac{S_{t_i}}{S_{t_{n+1}}} \left(\sum_{j=1}^{n+1} Z_j - y \right),$$

$i = 1, \dots, n$, where $S_{t_i} = A_1^{-2} + \dots + A_i^{-2}$.

iv. Set $B_i := F^{-1}(U_i + F(\theta_0)) \mod 2\pi$, $i = 1, \dots, n$.

Then (B_1, \dots, B_n) is distributed as $(\Theta_{t_1}, \dots, \Theta_{t_n}) | (\Theta_0 = \theta_0, \Theta_T = \theta_T)$.

The random vector (A_1, \dots, A_{n+1}) in Step 2 can, for instance, be simulated by an acceptance-rejection approach. A simple proposal density is the independent normal factor in (28), with $M_A := [\pi(y^2 + (T\sigma)^2)][T\sigma\sqrt{2\pi e}|y|]^{-1}$ being a (tight) bound for the first factor. Thus the efficiency of this acceptance-rejection algorithm is $1/M_A$. Figure 4 displays several jump-process bridge realizations simulated using Theorem 6.1.

Note that Steps *ii* and *iii* in Theorem 6.1 give an algorithm for simulating a discretized path (U_1, \dots, U_n) from the Cauchy bridge process $(V_{t_1}, \dots, V_{t_n}) | (V_0 = 0, V_T = y)$.

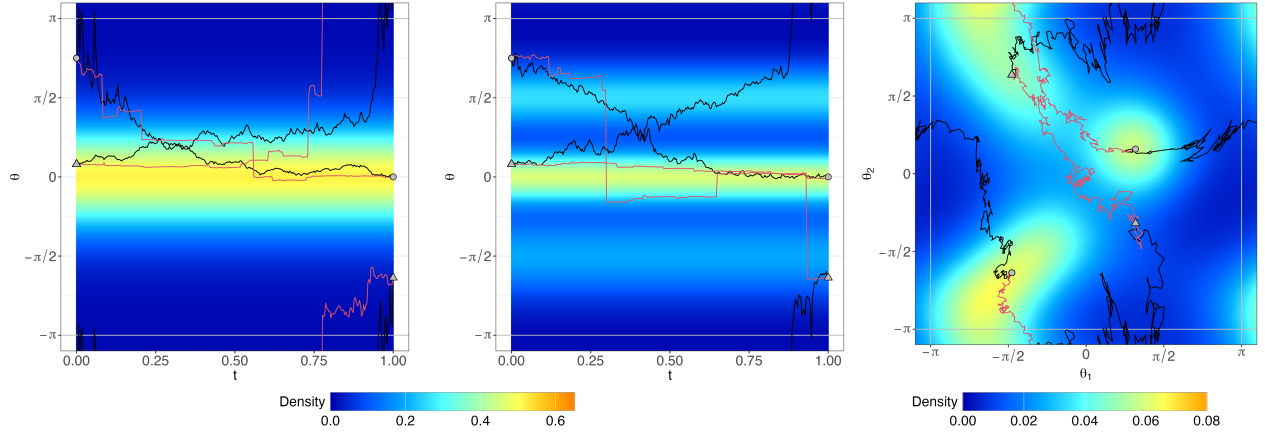


Figure 4: Simulated bridges in circular and toroidal processes, with overlaid stationary densities. The left and central plots show the $vM(0, 2)$ and $0.4vM(0, 8) + 0.3vM(-\pi/2, 3) + 0.3vM(\pi/2, 5)$ densities, respectively (see Figure 1). Here, black and red paths stand for diffusion and jump-process bridges, respectively. The right plot shows the $0.4BvM(-1.5, 2, 1, 1, -0.5) + 0.4BvM(-1.5, -2, 1, 1.5, 1) + 0.2BvM(1, 0.5, 2, 2, 0)$ density (see Figure 2). Here, all the paths are diffusion bridges. In all the plots, $\sigma = 0.15$ ($\Sigma = \sigma^2 I_2$) and $T = 1$.

7 Biological applications

7.1 Homogeneity of ant movements

In ant colonies, the ‘brood-to-worker ratio’ is defined as the number of brood items (larvae) divided by the number of workers (adult non-reproductive ants). This metric informs on the quality of care provided to the brood in a colony (Cassill and Tschinkel, 1999), which has been established as a relevant shaper of the offspring size (see, e.g., Purcell et al., 2012).

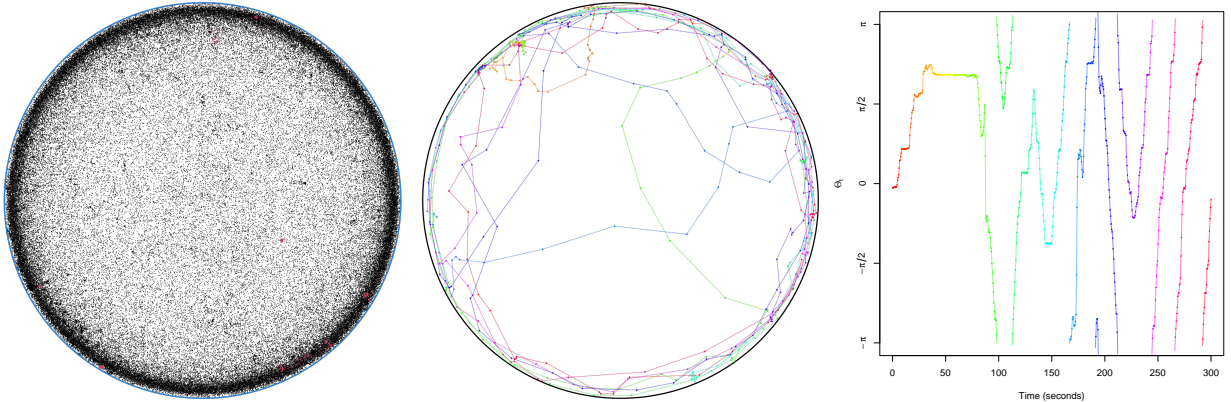


Figure 5: Left: Recorded coordinates of the 249 ants analysed along the first five minutes after being introduced in the circular arena (blue border). The red points indicate the eight ants that did not move in that time period. Centre: Recorded coordinates $\{(X_t, Y_t)\}$ of the track of a single ant. Right: Angles $\{\Theta_t\}$ of the ant with respect to the centre of the circular arena. The rainbow colour palette indicates the evolution of time and is shared between the last plots.

Sanmartín-Villar and Jeanson (2021) studied the effect of the brood-to-worker ratio during larval development in the behaviour of workers in the adult stage. Their study on *Lasius niger* ants involved raising ant larvae in nests with two brood-to-worker ratios: 3:1 (high brood treatment) and 1:3 (low brood treatment). Each of the callow workers that eclosed from the larvae was first exposed to the same social treatment: cohabitation with 22 mature workers in a Petri dish for 48 hours. After this period, the behavioural assays of the experiment took place. Each callow worker was put alone in a circular arena ($\varnothing = 5.8\text{cm}$, height = 1cm) covered with a glass lid and with walls coated with

a slippery substance. The ant was recorded on video and then its track coordinates were obtained with motion tracking software at a rate of 2.08 observations per second. Figure 5 (centre) shows the coordinates of the track of an ant in the circular arena.

As shown in Figure 5 (left and centre), ants tend to move on the periphery of the circular arena in a wall-following behaviour known as thigmotaxis. Thigmotaxis is a strategy used by ants to better orient themselves in the environment (Pratt et al., 2001; Dussutour et al., 2005). Due to this characteristic movement pattern, the sequence of ant coordinates in the arena $\{(X_t, Y_t)\}$ is well summarized by the sequence of angles $\{\Theta_t := \text{atan2}(Y_t, X_t)\}$ with respect to the centre of the arena, assumed as the origin.

We use von Mises diffusions to model $\{\Theta_t\}$ and conduct tests of homogeneity of the model parameters of k groups of diffusions (Theorem 4.2) for different factors derived from Sanmartín-Villar and Jeanson (2021)’s experiment: ‘brood treatment’ ($k = 2$ treatments: high and low, previously explained), ‘colony’ (the adults and larvae used in the experiment were extracted from $k = 3$ different colonies: A, B, and C), ‘size’ ($k = 2$ groups defined by the median) and ‘larval development’ ($k = 4$ groups induced by quartiles). ‘Larval development’ measured the number of days between egg and adult metamorphosis of a worker. Ants that undergo longer larval development are expected to reach adulthood with improved fitness levels. Splits of the ant size into more than two groups were highly unbalanced due to size repetitions, and thus discarded. The homogeneity tests serve to investigate whether the exploration behaviour of ants depends on the aforementioned factors.

We analyse the movements of the ants for the first five minutes of the first assay of the experiment, as this period could be assumed as the exploration stage of the ant within the new environment (e.g., Réale et al., 2007). Due to limitations of the tracking software, some ants have missing coordinates in their tracks. This occurred, for example, when an ant was shadowed by the walls of a Petri dish that is oblique to the lens of the recording camera. To avoid artefacts in the estimation of diffusion models, in our analysis we excluded ants with more than 5% missing data and imputed the missing coordinates of the remaining ants by linear interpolation on the coordinates $\{(X_t, Y_t)\}$. Eight ants were found to be (virtually) immobile during the considered time (red points in Figure 5) and therefore were excluded from the main analysis. The resulting preprocessed data are the discretized trajectories $\{\Theta_{\ell\Delta}^{(i,j)}\}_{\ell,j=0,1,1}^{n,N_j,k}$, with $n = 626$ and $\Delta = 0.48\text{s}$, and a total of $N_1 + \dots + N_k = 241$ ants.

Homogeneity	Brood	Colony	Size	Larval dev.
Means	1.0000	0.8363	1.0000	$4.9 \cdot 10^{-5}$
Concentrations	0.3376	1.0000	1.0000	0.0264
Volatilities	0.9096	1.0000	1.0000	0.1320
Stationary distrs.	0.1097	1.0000	1.0000	$1.2 \cdot 10^{-4}$
Concs. and volas.	0.3555	0.9096	1.0000	$5.8 \cdot 10^{-11}$
Diffusions	0.3376	1.0000	1.0000	$2.0 \cdot 10^{-11}$

Table 2: Corrected p -values of the tests of homogeneity of von Mises diffusions, for several types of hypotheses on $(\mu_j, \kappa_j, \sigma_j)$, $j = 1, \dots, k$, (rows) and different factors considered (columns). Correction is done with the false discovery rate method (Benjamini and Yekutieli, 2001).

Table 2 gives the corrected p -values of the k -sample tests for different homogeneity hypotheses. The groups of diffusions generated by the brood treatment ($N_{\text{high}} = 113$, $N_{\text{low}} = 128$) are not seen to be significantly different (lowest p -value: 0.1097). Therefore, no evidence of the impact of the brood-to-worker ratio in the exploration behaviour of ants, as proxied through the von Mises diffusion model fitted to the angular movement, is found. This conclusion is in line with those in Sanmartín-Villar and Jeanson (2021), where the brood treatment was found to not significantly affect ant behaviour metrics obtained from the coordinates of the tracks. The colony of origin ($N_A = 89$, $N_B = 68$, $N_C = 84$) and size ($N_1 = 100$, $N_2 = 136$; five sizes are missing) do not significantly affect the exploration behaviour of ants either. Finally, the ‘larval development’ of the ants is found to

affect the movement of ants, with the differences between groups being mostly attributed to different mean and concentration parameters.

The inclusion of immobile ants in the tests did not affect their decisions for ‘brood’ or ‘size’. For ‘colony’, however, this led to the rejection of several null hypotheses driven by the differences in the means (p -value: $3.1 \cdot 10^{-8}$), which is explainable by the fact that half of the immobile ants belong to Colony A. The effect of the inclusion of immobile ants in ‘larval development’ was a reduction in its p -values, with those for the homogeneity of concentrations and volatilities being $9.3 \cdot 10^{-5}$ and $4.9 \cdot 10^{-5}$, respectively.

To control the false discovery rate in the 48 tests conducted in the analysis, the method by Benjamini and Yekutieli (2001) was used to correct and report all the resulting p -values.

7.2 Protein structure bridging

The toroidal diffusion (8) and its exact bridge sampling can be applied to construct data-driven bridges between the backbones of two protein structures. The three-dimensional coordinates of the atoms in the main chain of a protein \mathbf{p} formed by N amino acids can essentially be parameterized as a sequence of pairs of dihedral angles $\{(\phi_i, \psi_i)\}_{i=1}^N \subset \mathbb{T}^2$. These angles describe the (sequential) relative positions between the planes formed by the atoms $C_{\alpha,i-1}-C'_{i-1}-N_i-C_{\alpha,i}$ and $C_{\alpha,i}-C'_i-N_{i+1}-C_{\alpha,i+1}$ of the polypeptide main chain formed by the repetition of the $N-C_{\alpha}-C'$ block. The i th amino acid side-chain is attached to $C_{\alpha,i}$, and (ϕ_i, ψ_i) are the rotation angles about the axes defined by the $N_i-C_{\alpha,i}$ and $C_{\alpha,i}-C'_i$ bonds, respectively (the angles ϕ_1 and ψ_N are undefined). The bond $C'-N$ is largely fixed due to its partial double bond nature, which generates the planar configurations of atoms. The dihedral-pairs representation is a parsimonious rotation-invariant parametrization of the backbone of a protein that, assuming ideal bond angles and lengths, captures essentially all the interesting variability in protein conformation (e.g., Richardson, 1981, p. 173). For two proteins \mathbf{p}_A and \mathbf{p}_B with $N = N_A = N_B$ (possibly different) amino acids, the relation between their three-dimensional main chains (which, in an abuse of notation, are also referred to as \mathbf{p}_A and \mathbf{p}_B in the sequel) is therefore essentially encoded in the tetra of dihedral angles $\{((\phi_{A,i}, \psi_{A,i}), (\phi_{B,i}, \psi_{B,i}))\}_{i=1}^N$.

Calmodulin (an abbreviation for CALcium MODULated proteIN) acts as an intermediary protein that senses calcium levels and relays signals to various calcium-sensitive enzymes, ion channels and other proteins (Dutta and Goodsell, 2003). Calmodulin has four Ca^{2+} binding sites, called EF-hands, that, when they are bound to calcium, transform the closed shape of the calcium-free calmodulin into an more open one. This shift of the three-dimensional protein structure is exemplified in the calcium-free calmodulin $\mathbf{p}_A \equiv \text{1cfd}$ (Kuboniwa et al., 1995), found in the African clawed frog (*Xenopus laevis*), and the Ca^{2+} -calmodulin $\mathbf{p}_B \equiv \text{1rfj}$ (Yun et al., 2004), found in the potato (*Solanum tuberosum*). Both proteins are $N = 148$ amino acids long, with coincidences in 133 amino acid sites (89.86%). We intend to simulate protein bridges between (the backbones of) \mathbf{p}_A and \mathbf{p}_B to emulate the transformation of the calmodulin in the presence of calcium and an alteration in its sequence of amino acids.

Our bridging between proteins \mathbf{p}_A and \mathbf{p}_B is based on three main steps: (i) for each amino acid site $i = 1, \dots, N$, learn a stationary density f_i to construct a toroidal diffusion (8); (ii) simulate dihedral bridges $\{(\Phi_i, \Psi_i)_{\nu\Delta}\}_{\nu=0, i=1}^{n, N}$ such that $(\Phi_i, \Psi_i)_0 = (\phi_{A,i}, \psi_{A,i})$ and $(\Phi_i, \Psi_i)_{n\Delta} = (\phi_{B,i}, \psi_{B,i})$, $i = 1, \dots, N$; (iii) invert the dihedral-pairs representation to merge these dihedral bridges into protein bridges between \mathbf{p}_A and \mathbf{p}_B . We elaborate on the details of each step next.

First, to learn a sensible stationary density f_i for the i th amino acid site we used the **top500** dataset, which contains 500 protein structures that are non-redundant and have been measured with a high precision (Word et al., 1999). For $i = 1, \dots, N$, we fitted a mixture of bivariate von Mises distributions \hat{f}_i using the subset **dih_i** of dihedral angles in the **top500** dataset whose amino acid is either $\text{aa}_{A,i}$ or $\text{aa}_{B,i}$, the respective amino acids of \mathbf{p}_A and \mathbf{p}_B in their i th sites. The estimate \hat{f}_i captures the particular toroidal density landscape in which the transition from $(\phi_{A,i}, \psi_{A,i})$ to $(\phi_{B,i}, \psi_{B,i})$ happens, with a possible change of amino acid involved. There are 42

unique `dihi` datasets, and their average size is 9,164 dihedral pairs. For each amino acid site, the bivariate von Mises mixtures were fit using Expectation-Maximization (EM) with the following procedure: (a) run EM fits for $m = 1, \dots, 20$ mixture components, initializing the algorithm with fast high-concentration Gaussian approximations (Mardia et al., 2007) and then using (numerical) maximum likelihood estimation of the bivariate von Mises parameters; (b) choose the number of components \hat{m} that gives the minimum BIC among 20 randomly-initialized EM fits for each m . The obtained \hat{m} range in [5, 19]. In (a), unimodality of the bivariate von Mises components was enforced to avoid identifiability issues. Additionally, \hat{f}_i was smoothed by truncating the largest concentration parameters to five. This smoothing is relevant to avoid simulated diffusion bridges with large jumps caused by extreme drifts or volatilities. Figure 6 shows the density contours of \hat{f}_i for the amino acid sites $i = 19, 41, 96, 135$, corresponding to the pairs of amino acids ($\text{aa}_{A,i}, \text{aa}_{B,i}$) being (Phenylalanine, Phenylalanine), (Glutamine, Glutamine), (Glycine, Glutamine), and (Glutamine, Glutamine), respectively.

Second, for the i th amino acid site we sampled diffusion bridges $\{(\Phi_i, \Psi_i)_{\nu\Delta}\}_{\nu=0,i=1}^{n,N}$ such that $(\Phi_i, \Psi_i)_0 = (\phi_{A,i}, \psi_{A,i})$ and $(\Phi_i, \Psi_i)_T = (\phi_{B,i}, \psi_{B,i})$, $i = 1, \dots, N$, for the diffusion (8) given by $(1 - \alpha)\hat{f}_i + \alpha/(2\pi)^2$ with a tuning parameter $\alpha \in [0, 1]$ that measures how ‘density-driven’ ($\alpha = 0$) or ‘shortest-path driven’ ($\alpha = 1$) is the diffusion bridge. We set $n = 113$ and $\Delta = 1/n$ (hence, $T = 1$), and $\sigma = 1/(2\pi)^2$. Figure 6 shows three simulated bridges between $(\phi_{A,i}, \psi_{A,i})$ and $(\phi_{B,i}, \psi_{B,i})$ for $i = 19, 41, 96, 135$, one for each $\alpha = 0.25, 0.5, 1$. While for $i = 19$ the pairs are relatively close and thus the simulated bridges follow a predictable path, for $i = 41$ the paths exploit the torus geometry and for $i = 96, 135$ are affected by the underlying density \hat{f}_i , which for $\alpha > 0$ significantly bends the Brownian bridges.

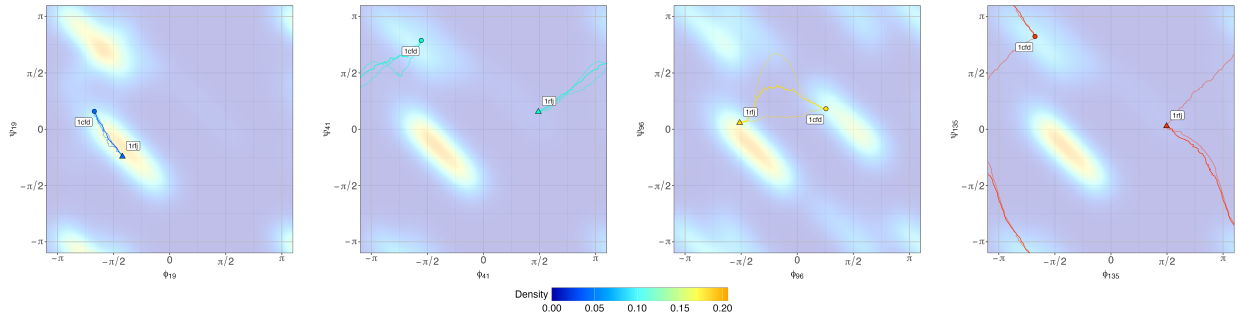


Figure 6: From left to right, the contour plots show the estimated density of the dihedral angle pairs for the amino acids Phenylalanine, Glutamine, Glycine and Glutamine, and Glutamine, respectively, in the `top500` dataset. These density estimates \hat{f}_i are used to build the toroidal diffusion for the amino acid sites $i = 19, 41, 96, 135$ of the proteins `1cfd` and `1rfj`. Three simulated diffusion bridges joining the i th dihedral angle pairs of these proteins are depicted; the path for $\alpha = 0.5$ is shown in solid colours and the two paths for $\alpha = 0.25, 1$ are shown with transparency.

Third and finally, we inverted the dihedral-pairs representation to obtain the three-dimensional protein backbone structures $\{P_{\nu\Delta}\}_{\nu=0}^n \subset \mathbb{R}^3$ from the dihedral bridges $\{(\Phi_1, \Psi_1, \dots, \Phi_N, \Psi_N)_{\nu\Delta}\}_{\nu=0}^n \subset \mathbb{T}^{2N}$. To construct $\{P_{\nu\Delta}\}_{\nu=0}^n$, we used first \mathbf{p}_A as structural basis (with its particular amino acid sequence) and modify its dihedral angles $\{(\phi_{A,i}, \psi_{A,i})\}_{i=1}^N$ according to the sampled dihedral bridges to reconstruct the three-dimensional structure, yielding $\{P_{A,\nu\Delta}\}_{\nu=0}^n$. After aligning the three-dimensional structure \mathbf{p}_B to that of \mathbf{p}_A , we obtained the time-reverted bridge $\{P_{B,(n-\nu)\Delta}\}_{\nu=0}^n$ analogously. These ‘forward’ and ‘backward’ bridges were merged with the linear interpolation (in \mathbb{R}^3) $P_{\nu\Delta} := (1 - \nu/n)P_{A,\nu\Delta} + (\nu/n)P_{B,(n-\nu)\Delta}$ in \mathbb{R}^3 to yield the advocated protein bridge. This symmetrization is applied to ensure that $P_0 = \mathbf{p}_A$ and $P_T = \mathbf{p}_B$, since due to the different amino acid sequences involved, the dihedral-pairs representation inversion yields $P_{A,T} \neq \mathbf{p}_B$ and $P_{B,T} \neq \mathbf{p}_A$. Figure 7 shows three simulated protein bridges between \mathbf{p}_A (top left) and \mathbf{p}_B (bottom right), and highlights with coloured spheres the positions of the amino acids whose dihedral bridges are shown in Figure 6.

The protein bridges shown in Figure 7 give simulated transformations of the closed shape of calcium-free calmodulin **1cfd** into the more open shape of the Ca^{2+} -calmodulin **1rfj**. In these simulated bridges, an opening of the protein backbone, much more marked than the open shape of **1rfj**, is followed by an elongation of the backbone and then a contraction to converge to **1rfj**. Along this opening and closing of the protein structure, large torsions at certain parts of the main chain take place. For example, between the protein begin and the blue ball (amino acid sites 1–19), five amino acid sites concentrate the large torsions, and between the blue and cyan spheres (20–41), eleven sites 20–41 concentrate the main torsions. The unfolding of the protein backbone is more marked for $\alpha = 0.25$ and less for $\alpha = 1$.

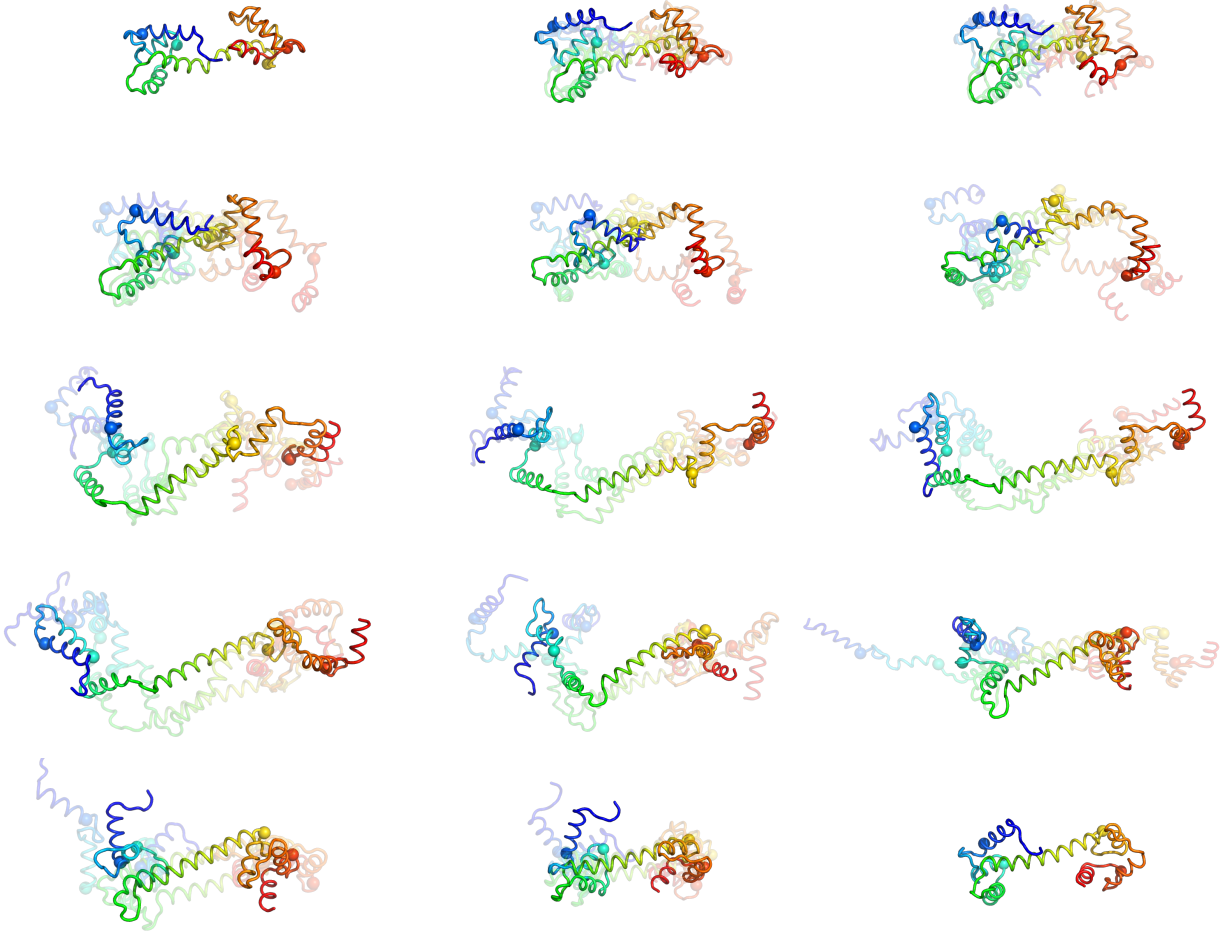


Figure 7: From top to bottom and left to right, each figure represents a temporal snapshot of the three simulated protein bridges between the main chains of the proteins **1cfd** and **1rfj** according to the diffusion bridge described in Section 5. The 15 snapshots are at equidistant time points between the begin (**1cfd**, top left corner) and end (**1rfj**, bottom right corner) of the simulated bridges. The simulated trajectories shown with transparency correspond to $\alpha = 0.25, 1$, while the one shown in solid colours represents $\alpha = 0.5$. The coloured spheres signal the positions of the amino acid sites 19, 41, 96, and 135. The corresponding three simulated dihedral bridges for these amino acids are shown in Figure 6. The figure was prepared with PyMOL (Schrödinger, LLC, 2022).

The present application gives a proof of concept on how toroidal diffusion bridges (8) can be utilized to create protein bridges from estimated densities of pairs of dihedral angles. Further

potential applications of these protein bridges include the simulation of the folding process of a protein \mathbf{p} from its idealistic linear state with $\phi_i = \psi_i = 0$, $i = 1, \dots, N$, to its folded state, or their use as stochastic interpolators in molecular dynamics simulations, allowing to refine to a higher temporal resolution a time series of protein structures $\mathbf{p}_{t_0}, \dots, \mathbf{p}_{t_n}$.

Several limitations exist in the proposed protein bridges that warrant further research. An important one is the independence between the diffusion processes associated with different amino acids and shared volatilities, which may induce intermediate unfolded shapes that are unrealistic. Dependence between diffusions could be introduced with a hidden Markov model that creates a density estimate on \mathbb{T}^{2N} tailored to the amino acids in \mathbf{p}_A and \mathbf{p}_B , as explored in Golden et al. (2017). Additional challenges include avoiding potential atom clashes in intermediate backbones, and managing insertions and deletions of amino acids to handle proteins \mathbf{p}_A and \mathbf{p}_B with $N_A \neq N_B$. This last issue is needed to use these protein bridges to model protein structural evolution processes. In this regard, the presented bridges are time-reversible, aligning with the Pulley principle commonly considered in evolutionary trees (Felsenstein, 1981).

Acknowledgement

The first author acknowledges support from grant PID2021-124051NB-I00, funded by MCIN/AEI/-10.13039/50110001103 and by “ERDF A way of making Europe”. His research was also supported by “Convocatoria de la Universidad Carlos III de Madrid de Ayudas para la recualificación del sistema universitario español para 2021–2023”, funded by Spain’s Ministerio de Ciencia, Innovación y Universidades. Part of this work was developed during the Oberwolfach workshop “Statistics of Stochastic Differential Equations on Manifolds and Stratified Spaces”; both authors gratefully acknowledge the hospitality of the organizers and MFO. Part of the simulations were conducted at the Centro de Supercomputación de Galicia (CESGA). The authors appreciate data availability from Dr. Iago Sanmartín-Villar, as well as insightful discussions, regarding the application in Section 7.1. The authors also appreciate discussions with Prof. Thomas Hamelryck and Prof. Jotun Hein regarding the application in Section 7.2.

References

- Applebaum, D. (2009). *Lévy Processes and Stochastic Calculus*, volume 116 of *Cambridge Studies in Advanced Mathematics*. Cambridge University Press, Cambridge, second edition.
- Benjamini, Y. and Yekutieli, D. (2001). The control of the false discovery rate in multiple testing under dependency. *Ann. Stat.*, 29(4):1165–1188.
- Breckling, J. (1989). *The Analysis of Directional Time Series: Applications to Wind Speed and Direction*, volume 61 of *Lecture Notes in Statistics*. Springer, London.
- Cassill, D. L. and Tschinkel, W. R. (1999). Effects of colony-level attributes on larval feeding in the fire ant, *Solenopsis invicta*. *Insectes Soc.*, 46(3):261–266.
- Codling, E. A. and Hill, N. A. (2005). Calculating spatial statistics for velocity jump processes with experimentally observed reorientation parameters. *J. Math. Biol.*, 51(5):527–556.
- Dussutour, A., Deneubourg, J.-L., and Fourcassié, V. (2005). Temporal organization of bi-directional traffic in the ant *Lasius niger* (L.). *J. Exp. Biol.*, 208(15):2903–2912.
- Dutta, S. and Goodsell, D. S. (2003). Molecule of the month: Calmodulin. RCSB Protein Data Bank. Accessed: 2024-08-24.

- Felsenstein, J. (1981). Evolutionary trees from DNA sequences: A maximum likelihood approach. *J. Mol. Evol.*, 17(6):368–376.
- Feng, Z. and McCulloch, C. E. (1992). Statistical inference using maximum likelihood estimation and the generalized likelihood ratio when the true parameter is on the boundary of the parameter space. *Stat. Probab. Lett.*, 13(4):325–332.
- Fisher, N. I. and Lee, A. J. (1994). Time series analysis of circular data. *J. R. Stat. Soc. Ser. B Methodol.*, 56(2):327–339.
- Forman, J. L. and Sørensen, M. (2014). A transformation approach to modelling multi-modal diffusions. *J. Stat. Plan. Inference*, 146:56–69.
- Frank, T. D. (2005). *Nonlinear Fokker–Planck Equations*. Springer Series in Synergetics. Springer-Verlag, Berlin.
- García-Portugués, E., Sørensen, M., Mardia, K. V., and Hamelryck, T. (2019). Langevin diffusions on the torus: estimation and applications. *Stat. Comput.*, 29(1):1–22.
- Golden, M., García-Portugués, E., Sørensen, M., Mardia, K. V., Hamelryck, T., and Hein, J. (2017). A generative angular model of protein structure evolution. *Mol. Biol. Evol.*, 34(8):2085–2100.
- Harvey, A., Hurn, S., Palumbo, D., and Thiele, S. (2024). Modelling circular time series. *J. Econom.*, 239(1):105450.
- Hill, N. A. and Häder, D.-P. (1997). A biased random walk model for the trajectories of swimming micro-organisms. *J. Theor. Biol.*, 186(4):503–526.
- Jacod, J. and Sørensen, M. (2018). A review of asymptotic theory of estimating functions. *Stat. Inference Stoch. Process.*, 21(2):415–434.
- Kato, S. and Pewsey, A. (2015). A Möbius transformation-induced distribution on the torus. *Biometrika*, 102(2):359–370.
- Kent, J. T. (1975). Discussion of “Statistics of directional data”. *J. R. Stat. Soc. Ser. B Methodol.*, 37(3):377–378.
- Kuboniwa, H., Tjandra, N., Grzesiek, S., Ren, H., Klee, C. B., and Bax, A. (1995). Solution structure of calcium-free calmodulin. *Nat. Struct. Mol. Biol.*, 2(9):768–776.
- Mardia, K. V., Taylor, C. C., and Subramaniam, G. K. (2007). Protein bioinformatics and mixtures of bivariate von Mises distributions for angular data. *Biometrics*, 63(2):505–512.
- Øksendal, B. (2003). *Stochastic Differential Equations*. Universitext. Springer-Verlag, Berlin, sixth edition.
- Pewsey, A. and García-Portugués, E. (2021). Recent advances in directional statistics. *Test*, 30(1):1–58.
- Pratt, S. C., Brooks, S. E., and Franks, N. R. (2001). The use of edges in visual navigation by the ant *Leptothorax albipennis*. *Ethology*, 107(12):1125–1136.
- Purcell, J., Brüttsch, T., and Chapuisat, M. (2012). Effects of the social environment on the survival and fungal resistance of ant brood. *Behav. Ecol. Sociobiol.*, 66(3):467–474.
- Réale, D., Reader, S. M., Sol, D., McDougall, P. T., and Dingemanse, N. J. (2007). Integrating animal temperament within ecology and evolution. *Biol. Rev.*, 82(2):291–318.

- Richardson, J. S. (1981). The anatomy and taxonomy of protein structure. volume 34 of *Advances in Protein Chemistry*, pages 167–339. Academic Press.
- Roberts, G. O. and Stramer, O. (2002). Langevin diffusions and Metropolis–Hastings algorithms. *Methodol. Comput. Appl. Probab.*, 4(4):337–357.
- Rosenblatt, M. (1952). Remarks on a multivariate transformation. *Ann. Math. Stat.*, 23:470–472.
- Sanmartín-Villar, I. and Jeanson, R. (2021). Early social context does not influence behavioral variation at adulthood in ants. *Curr. Zool.*, 68(3):335–344.
- Schrödinger, LLC (2022). The PyMOL molecular graphics system, version 2.5.4.
- Silvey, S. D. (1970). *Statistical Inference*. Library of University Mathematics. Penguin Books, Baltimore.
- Singh, H., Hnizdo, V., and Demchuk, E. (2002). Probabilistic model for two dependent circular variables. *Biometrika*, 89(3):719–723.
- Sørensen, M. (2012). Estimating functions for diffusion-type processes. In Kessler, M., Lindner, A., and Sørensen, M., editors, *Statistical Methods for Stochastic Differential Equations*, volume 124 of *Monographs on Statistics and Applied Probability*, pages 1–107. CRC Press, Boca Raton.
- Wehrly, T. E. and Johnson, R. A. (1980). Bivariate models for dependence of angular observations and a related Markov process. *Biometrika*, 67(1):255–256.
- Word, J. M., Lovell, S. C., LaBean, T. H., Taylor, H. C., Zalis, M. E., Presley, B. K., Richardson, J. S., and Richardson, D. C. (1999). Visualizing and quantifying molecular goodness-of-fit: small-probe contact dots with explicit hydrogen atoms. *J. Mol. Biol.*, 285(4):1711–1733.
- Yun, C.-H., Bai, J., Sun, D.-Y., Cui, D.-F., Chang, W.-R., and Liang, D.-C. (2004). Structure of potato calmodulin PCM6: the first report of the three-dimensional structure of a plant calmodulin. *Acta Crystallogr. D*, 60(7):1214–1219.

A Proofs

Proof of Proposition 2.1. Set $g(x) := F^{-1}(x + F(\theta_0))$, $\theta_0 \in \mathbb{T}^1$. Then $g'(x) = 1/f(g(x))$ and $g''(x) = -f'(g(x))/f(g(x))^3$. Taking $X_t := g(\sigma W_t)$ and applying Itô’s formula yields

$$dX_t = \frac{\sigma^2}{2} g''(W_t) dt + g'(W_t) \sigma dW_t = -\frac{\sigma^2 f'(X_t)}{2f(X_t)^3} dt + \frac{\sigma}{f(X_t)} dW_t. \quad (29)$$

Therefore, X_t is the solution of (2), and hence Θ_t is by definition the solution of (3). The density of $X_{t_2} | X_{t_1} = x_1$, denoted by $p_{t_2-t_1}^X$, follows by a direct transformation of variables:

$$p_{t_2-t_1}^X(x_2 | x_1) = \phi_{(t_2-t_1)\sigma^2}(F(x_2) - F(x_1))f(x_2), \quad x_1, x_2 \in \mathbb{R}.$$

Consider a random variable $\Phi := m(X)$, $X \sim f_X$, where $m(x) := x \bmod 2\pi \in \mathbb{T}^1$, $x \in \mathbb{R}$, is a many-to-one function. The restriction $m_k := m|_{I_k}$, with $I_k = [2k\pi, 2(k+1)\pi)$ and $k \in \mathbb{Z}$, has inverse $m_k^{-1}(\phi) = \phi + 2k\pi$, $\phi \in \mathbb{T}^1$. Hence, the density of Φ is given by

$$f_\Phi(\phi) = \sum_{k \in \mathbb{Z}} f_X(m_k^{-1}(\phi)) \frac{d}{dy} m_k^{-1}(\phi) = \sum_{k \in \mathbb{Z}} f_X(\phi + 2k\pi), \quad \phi \in \mathbb{T}^1. \quad (30)$$

After wrapping the diffusion, the density of $\Theta_{t_2} \mid X_{t_1} = x_1$, denoted by $p_{t_2-t_1}^{\Theta, X}$, becomes

$$p_{t_2-t_1}^{\Theta, X}(\theta_2 \mid x_1) = \sum_{k \in \mathbb{Z}} p_{t_2-t_1}^X(\theta_2 + 2k\pi \mid x_1) = \sum_{k \in \mathbb{Z}} \phi_{(t_2-t_1)\sigma^2}(F(\theta_2) + k - F(x_1))f(\theta_2), \quad \theta_2 \in \mathbb{T}^1.$$

Now, for $\theta \in \mathbb{T}^1$, $p_{t_2-t_1}^{\Theta, X}(\theta_2 \mid \theta_1 + 2m\pi) = p_{t_2-t_1}^{\Theta, X}(\theta_2 \mid \theta_1)$, which implies that the distribution of $\Theta_{t_2} \mid \Theta_{t_1} = \theta_1$ equals that of $\Theta_{t_2} \mid X_{t_1} = \theta_1$. Thus, the transition probability density of the circular diffusion (3), $p_{t_2-t_1}$, is

$$p_{t_2-t_1}(\theta_2 \mid \theta_1) = 2\pi f_{\text{WN}}(2\pi F(\theta_2); 2\pi F(\theta_1), 4\pi^2(t_2 - t_1)\sigma^2)f(\theta_2).$$

Because $f_{\text{WN}}(\theta; \mu, \sigma^2)$ converges to the uniform density on \mathbb{T}^1 as $\sigma^2 \rightarrow \infty$, it follows that

$$\lim_{t \rightarrow \infty} p_t(\theta \mid \theta_0) = f(\theta) 2\pi \lim_{t \rightarrow \infty} f_{\text{WN}}(2\pi F(\theta); 2\pi F(\theta_0), 4\pi^2 t \sigma^2) = f(\theta)$$

for any $\theta, \theta_0 \in \mathbb{T}^1$. The result concerning f_{WN} can be readily verified, e.g., by exploiting the Fourier form of the wrapped normal density: $f_{\text{WN}}(\theta; \mu, \sigma^2) = \frac{1}{2\pi} \{1 + 2 \sum_{k=1}^{\infty} e^{-k\sigma} \cos(k(\theta - \mu))\}$. This shows that $\{\Theta_t\}$ is ergodic with stationary density f . Finally, it readily follows that $\{\Theta_t\}$ is time-reversible since $p_{t_2-t_1}(\theta_2 \mid \theta_1)/p_{t_2-t_1}(\theta_1 \mid \theta_2) = f(\theta_2)/f(\theta_1)$ because $f_{\text{WN}}(x; y, \sigma^2) = f_{\text{WN}}(y; x, \sigma^2)$ for $x, y \in \mathbb{R}$. \square

Proof of Proposition 3.1. We prove the first two statements, as the remaining ones follow analogously to the proof of Proposition 2.1. We use the multidimensional Itô formula (e.g., Øksendal, 2003, p. 48). Let $\mathbf{V}_t := \Sigma^{1/2} \mathbf{W}_t$ and $\mathbf{X}_t := g(\mathbf{V}_t)$ for a C^2 -function $g : \mathbb{R}^p \rightarrow \mathbb{R}^p$. Then, for $k = 1, \dots, p$,

$$dX_{k,t} = \frac{1}{2} \sum_{i,j=1}^p \frac{\partial^2 g_k(\mathbf{V}_t)}{\partial x_i \partial x_j} \Sigma_{i,j} dt + \sum_{i=1}^p \frac{\partial g_k(\mathbf{V}_t)}{\partial x_i} dV_{i,t} = \frac{1}{2} \text{tr}[\Sigma H g_k(\mathbf{V}_t)] dt + \nabla g_k(\mathbf{V}_t) \Sigma^{1/2} d\mathbf{W}_t$$

and therefore

$$d\mathbf{X}_t = \frac{1}{2} \begin{pmatrix} \text{tr}[\Sigma(Hg_1)(g^{-1}(\mathbf{X}_t))] \\ \vdots \\ \text{tr}[\Sigma(Hg_p)(g^{-1}(\mathbf{X}_t))] \end{pmatrix} dt + (Dg)(g^{-1}(\mathbf{X}_t)) \Sigma^{1/2} d\mathbf{W}_t.$$

Setting $g(\mathbf{x}) := R^{-1}(\mathbf{x} + R(\boldsymbol{\theta}_0))$, $\boldsymbol{\theta}_0 \in \mathbb{T}^p$, and $\boldsymbol{\Theta}_t := g(\Sigma^{1/2} \mathbf{W}_t) \bmod 2\pi$ proves the first statement. The density of $\mathbf{X}_{t_2} \mid \mathbf{X}_{t_1} = \mathbf{x}_1$, denoted by $p_{t_2-t_1}^{\mathbf{X}}$, follows by the transformation theorem as

$$p_{t_2-t_1}^{\mathbf{X}}(\mathbf{x}_2 \mid \mathbf{x}_1) = \phi_{(t_2-t_1)\Sigma}(R(\mathbf{x}_2) - R(\mathbf{x}_1))f(\mathbf{x}_2), \quad \mathbf{x}_1, \mathbf{x}_2 \in \mathbb{R}^p,$$

because $|\partial R(\mathbf{x})/\partial \mathbf{x}| = f_1(x_1)f_2(x_2 \mid x_1) \cdots f_p(x_p \mid x_1, \dots, x_{p-1}) = f(\mathbf{x})$. Analogously to the proof of Proposition 2.1, it follows that the transition probability density of the toroidal diffusion (7), $p_{t_2-t_1}$, is

$$p_{t_2-t_1}(\boldsymbol{\theta}_2 \mid \boldsymbol{\theta}_1) = (2\pi)^p f_{\text{WN}}(2\pi R(\boldsymbol{\theta}_2); 2\pi R(\boldsymbol{\theta}_1), 4\pi^2(t_2 - t_1)\Sigma)f(\boldsymbol{\theta}_2)$$

and that the process is time-reversible and ergodic with stationary density f . \square

Proof of Theorem 4.1. The first claim of the theorem follows from general results for estimating functions for ergodic stochastic processes in Theorem 3.2 in Jacod and Sørensen (2018). Using basic calculus results and doing long and tedious calculations, it can be checked that under the conditions of the theorem, the estimating function $n^{-1} \partial_{\boldsymbol{\xi}} \ell_n(\boldsymbol{\xi})$, i.e., a normalized version of the score function given by (13), satisfies Condition 3.1 in Jacod and Sørensen (2018). The compactness

of \mathbb{T}^1 is essential. In particular, it can be established that the classical interchange of integration and differentiation, which proves that $E_{\xi_0}(\partial_{\xi}^2 \log p_{\Delta}(\Theta_{2\Delta}; \xi_0 \mid \Theta_{\Delta})) = -\mathcal{I}^{\Delta}(\xi_0)$, is allowed.

The asymptotic normality follows by standard arguments, see Theorem 2.11 in Jacod and Sørensen (2018), from the central limit theorem for martingales, by which

$$n^{-1/2} \partial_{\xi} \ell_n(\xi_0) \xrightarrow{\mathcal{D}} \mathcal{N}_q(\mathbf{0}, \mathcal{I}^{\Delta}(\xi_0)). \quad (31)$$

That the score function is a martingale follows by an interchange of differentiation and integration (see, e.g., Sørensen, 2012, p. 11), which can be shown to be allowed under the conditions of the theorem. By the ergodic theorem, $\mathcal{I}_n^{\Delta}(\xi_0)$ converges in probability to $\mathcal{I}^{\Delta}(\xi_0)$. By arguments similar to those given in the proof of Theorem 3.2 in Jacod and Sørensen (2018), it can be proved that the convergence of $\mathcal{I}_n^{\Delta}(\xi)$ is uniform for ξ in a compact subset of Ξ containing ξ_0 . Thus $\mathcal{I}_n^{\Delta}(\hat{\xi}_n)$ converges to $\mathcal{I}^{\Delta}(\xi_0)$.

Finally, (17) follows by standard arguments involving Taylor expansions; see, e.g., Silvey (1970). It is needed that $-n^{-1} \ddot{\ell}_n(\hat{\xi}_n) \xrightarrow{\mathbb{P}_{\xi_0}} \mathcal{I}^{\Delta}(\xi_0)$, where $\ddot{\ell}_n(\xi)$ denotes the Hessian of ℓ_n . This is true because $n^{-1} \ddot{\ell}_n(\xi)$ converges uniformly for ξ in a compact set (see the proof of Theorem 3.2 in Jacod and Sørensen (2018)), and $-n^{-1} \ddot{\ell}_n(\xi_0) \xrightarrow{\mathbb{P}_{\xi_0}} \mathcal{I}^{\Delta}(\xi_0)$. In this way, it is found that $-2 \log Q_n = \dot{\ell}_n(\xi_0)' / \sqrt{n} \mathcal{I}^{\Delta}(\xi_0)^{-1/2} [\mathbf{I}_q - \mathbf{R}] [\mathbf{I}_q - \mathbf{R}] \mathcal{I}^{\Delta}(\xi_0)^{-1/2} \dot{\ell}_n(\xi_0) / \sqrt{n} + o_P(1)$, where $\mathbf{R} = \mathcal{I}^{\Delta}(\xi_0)^{1/2} \mathcal{K}(\xi_0) \mathcal{I}^{\Delta}(\xi_0)^{1/2}$. Here $\mathcal{K}(\xi_0)$ denotes the matrix with the upper left corner equal to $\mathcal{I}^{\Delta}(\xi_0)_{11}^{-1}$ with $\mathcal{I}^{\Delta}(\xi_0)_{11}$ denoting the upper left $q_1 \times q_1$ -corner of the Fisher information matrix. Since \mathbf{R} is idempotent of rank q_1 , it follows that $\mathbf{I}_q - \mathbf{R}$ is the orthogonal projection on a subspace of dimension q_2 . Thus the last result of the theorem follows from (31). \square

Proof of Theorem 4.2. As in the proof Theorem 4.1 the result follows from general results in Jacod and Sørensen (2018) and Taylor expansions. First, we need to show that, as $n_i N_i \rightarrow \infty$, $i = 1, \dots, k$,

$$D_{n,N}^{-1/2} \partial_{\xi} \ell_{n,N}(\xi_0) \xrightarrow{\mathcal{D}} \mathcal{N}_{kq}(\mathbf{0}, \mathcal{J}(\xi_0)), \quad (32)$$

and $D_{n,N}^{-1} \ddot{\ell}_{n,N}(\xi) = D_{n,N}^{-1/2} \ddot{\ell}_{n,N}(\xi) D_{n,N}^{-1/2}$ converges uniformly for ξ in a compact set with limit $\mathcal{J}(\xi_0)$ for the true parameter value ξ_0 . Here $D_{n,N} = \text{diag}(n_1 N_1, \dots, n_1 N_1, \dots, n_k N_k, \dots, n_k N_k)$ with each $n_j N_j$ repeated q times, while the Fisher information $\mathcal{J}(\xi)$ is the block-diagonal matrix $\mathcal{J}(\xi) = \text{diag}(\mathcal{I}^{\Delta_1}(\xi), \dots, \mathcal{I}^{\Delta_k}(\xi))$.

The assumption $n_i N_i \rightarrow \infty$ implies that either $n_i \rightarrow \infty$ or $N_i \rightarrow \infty$. For a group where $n_i \rightarrow \infty$, we can consider N_i fixed and use that in the proof of Theorem 4.1 we have shown that the score function for each observed trajectory is a martingale and checked Condition 3.1 in Jacod and Sørensen (2018). Therefore we have previously established the limit results for the individual trajectories, and by independence the limit results follow for the group of trajectories.

For a group where $N_i \rightarrow \infty$, we can consider n_i fixed, and for this longitudinal data setting, we can use results in Section 4 in Jacod and Sørensen (2018). In our setting Condition 4.1 of that paper is essentially identical to Condition 3.1, which we checked in the proof of Theorem 4.1. Therefore, the limit results follows for such a group by the law of large numbers for i.i.d. variables, see the proof of Theorem 4.1 of Jacod and Sørensen (2018). Thus the limit results have been established for all groups, and hence it follows that they hold for the score function of the entire data set.

Under the assumptions of the theorem, $D_0 := \lim(n_1 N_1)^{-1} D_{n,N}$ exists, and we can define $\tilde{M} = D_0^{1/2} M$ and $\mathcal{K}(\xi_0) = \tilde{M} (\tilde{M}' \mathcal{J}(\xi_0) \tilde{M})^{-1} \tilde{M}'$. By Taylor expansions and the second limit result above it is found that $D_{n,N}^{1/2} (\hat{\xi} - \xi_0) = \mathcal{J}(\xi_0) D_{n,N}^{-1/2} \partial_{\xi} \ell_{n,N}(\xi_0) + o_P(1)$ and $D_{n,N}^{1/2} (\hat{\xi}_M - \xi_0) = \mathcal{K}(\xi_0) D_{n,N}^{-1/2} \partial_{\xi} \ell_{n,N}(\xi_0) + o_P(1)$, where $\hat{\xi}_M$ denotes the maximum likelihood estimator under the hypothesis $\xi \in MA$. By further expansions we find that $-2 \log Q_{n,N} = (D_{n,N}^{-1/2} \dot{\ell}_{n,N}(\xi_0))' \mathcal{J}(\xi_0)^{-1/2} [\mathbf{I}_{kq} - \mathbf{R}] [\mathbf{I}_{kq} - \mathbf{R}] \mathcal{J}(\xi_0)^{-1/2} D_{n,N}^{-1/2} \dot{\ell}_{n,N}(\xi_0) / \sqrt{n} + o_P(1)$ with $\mathbf{R} = \mathcal{J}(\xi_0)^{1/2} \mathcal{K}(\xi_0) \mathcal{J}(\xi_0)^{1/2}$. Since \mathbf{R} is idempotent of rank \tilde{q} , it follows that $\mathbf{I}_{kq} - \mathbf{R}$ is the orthogonal projection on a subspace of

dimension $kq - \tilde{q}$. Thus (21) follows from (32). \square

Proof of Theorem 5.1. By Proposition 3.1, $\Theta_t = h(\mathbf{W}_t)$, where $h(\mathbf{x}) := R^{-1}(\Sigma^{1/2}\mathbf{x} + R(\theta_0)) \bmod 2\pi$, and $\{\mathbf{W}_t\}$ is a standard Wiener process (in particular $\mathbf{W}_0 = \mathbf{0}$). Note that $\Theta_0 = \theta_0$. The condition $\Theta_T = \theta_T$ is equivalent to $\mathbf{W}_T = \Sigma^{-1/2}[R(\theta_T + 2\mathbf{k}_T\pi) - R(\theta_0)] = \Sigma^{-1/2}[R(\theta_T) - R(\theta_0) + \mathbf{k}_T]$, with \mathbf{k}_T in \mathbb{Z}^p . Let $\mathbf{y}_\mathbf{k} := \Sigma^{-1/2}(R(\theta_T) - R(\theta_0) + \mathbf{k})$, $\mathbf{k} \in \mathbb{Z}^p$, and let $A_i \subset \mathbb{T}^p$, $i = 1, \dots, n$, be arbitrary Borel sets. Then:

$$\begin{aligned} \mathbb{P}[\Theta_{t_1} \in A_1, \dots, \Theta_{t_n} \in A_n \mid \Theta_T = \theta_T] \\ &= \sum_{\mathbf{k} \in \mathbb{Z}^p} \mathbb{P}[\Theta_{t_1} \in A_1, \dots, \Theta_{t_n} \in A_n \mid \mathbf{K}_T = \mathbf{k}, \Theta_T = \theta_T] \times \mathbb{P}[\mathbf{K}_T = \mathbf{k} \mid \Theta_T = \theta_T] \\ &= \sum_{\mathbf{k} \in \mathbb{Z}^p} \mathbb{P}[h(\mathbf{W}_{t_1}) \in A_1, \dots, h(\mathbf{W}_{t_n}) \in A_n \mid \mathbf{W}_T = \mathbf{y}_\mathbf{k}] \times \mathbb{P}[\mathbf{K}_T = \mathbf{k} \mid \Theta_T = \theta_T], \end{aligned}$$

where we have used that the events $\{\mathbf{K}_T = \mathbf{k}, \Theta_T = \theta_T\}$ and $\{\mathbf{W}_T = \mathbf{y}_\mathbf{k}\}$ are the same. It is not difficult to see that $\mathbb{P}[\mathbf{K}_T = \mathbf{k} \mid \Theta_T = \theta_T]$ equals the right hand side of (24). The theorem therefore follows because the distribution of (U_1, \dots, U_n) (constructed in Step *ii*) equals the conditional distribution $(\mathbf{W}_{t_1}, \dots, \mathbf{W}_{t_n}) \mid \mathbf{W}_T = \mathbf{y}_\mathbf{k}$. \square

Proof of Theorem 6.1. The theorem is proved in the same way as Theorem 5.1. The main difference is that it must be proved that the distribution of (U_1, \dots, U_n) (constructed in Steps *ii* and *iii*) equals the conditional distribution $(V_{t_1}, \dots, V_{t_n}) \mid V_T = y$, where $\{V_t\}$ is a Cauchy process with scale parameter σ .

The process $V_t = \tilde{W}_{S_t}$, where $\{\tilde{W}_t\}$ and $\{S_t\}$ are as explained above the theorem, is a (symmetric) Cauchy process with scale parameter σ . Let A_1, \dots, A_{n+1} be independent $\mathcal{N}(0, 2\Delta_i^{-2})$ -distributed random variables. Then we can simulate the increments of $\{S_t\}$ by $S_{t_i} - S_{t_{i-1}} = A_i^{-2}$, $i = 1, \dots, n+1$, where $S_0 = 0$ by definition. With a slight abuse of notation, we denote the density of $V_{t_1}, \dots, V_{t_{n+1}}, A_1, \dots, A_{n+1}$ by $f(v_1, \dots, v_{n+1}, a_1, \dots, a_{n+1})$, and similarly for other densities. Then the density of the bridge $V_{t_1}, \dots, V_{t_n} \mid V_{t_{n+1}} = v_{n+1}$ is

$$\begin{aligned} f(v_1, \dots, v_n \mid v_{n+1}) &= \int_{(0, \infty)^{n+1}} f(v_1, \dots, v_n, a_1, \dots, a_{n+1} \mid v_{n+1}) da_1 \cdots da_{n+1} \\ &= \int_{(0, \infty)^{n+1}} f(v_1, \dots, v_n \mid a_1, \dots, a_{n+1}, v_{n+1}) f(a_1, \dots, a_{n+1} \mid v_{n+1}) da_1 \cdots da_{n+1}. \end{aligned}$$

The first factor under the integral is the density of a Brownian bridge with infinitesimal variance $2\sigma^2$ observed at the time points $\tau_i = A_1^{-2} + \dots + A_i^{-2}$, $i = 1, \dots, n$ (simulated in Step *iii*). By Bayes' formula

$$\begin{aligned} f(a_1, \dots, a_{n+1} \mid v_{n+1}) &= f(v_{n+1} \mid a_1, \dots, a_{n+1}) f(a_1, \dots, a_{n+1}) / f(v_{n+1}) \\ &= \frac{\phi_{2\sigma^2(a_1^{-2} + \dots + a_{n+1}^{-2})}(v_{n+1})}{f_C(v_{n+1}; 0, (t_{n+1}\sigma)^2)} \prod_{i=1}^{n+1} \phi_{2\Delta_i^{-2}}(a_i). \end{aligned}$$

Thus A_1, \dots, A_{n+1} in Step *ii* is drawn from the conditional distribution given by the second factor under the second integral above with $v_{n+1} = y$. In conclusion, the vector (U_1, \dots, U_n) is a draw from the distribution of the Cauchy bridge $(V_{t_1}, \dots, V_{t_n}) \mid V_T = y$. \square